Quaternary Science Reviews 196 (2018) 177–192

Contents lists available at ScienceDirect

Quaternary Science Reviews

journal homepage: www.elsevier.com/locate/quascirev

Holocene sea-level database from the Atlantic coast of Europe

Ane García-Artola [a, b, *], Pierre Stéphan [c], Alejandro Cearreta [a, d], Robert E. Kopp [e], Nicole S. Khan [b], Benjamin P. Horton [b, f]

[a] Departamento de Estratigrafía y Paleontología, Universidad del País Vasco UPV/EHU, Bilbao, Spain
[b] Asian School of the Environment, Nanyang Technological University, Singapore
[c] CNRS, Laboratoire LETG, Institut Universitaire Européen de la Mer, Université de Bretagne Occidentale, Plouzané, France
[d] Basque Centre for Climate Change-BC3, Leioa, Spain
[e] Department of Earth and Planetary Sciences and Institute of Earth, Ocean and Atmospheric Sciences, Rutgers University, New Brunswick, NJ, USA
[f] Earth Observatory of Singapore, Nanyang Technological University, Singapore

A R T I C L E I N F O

Article history:
Received 29 March 2018
Received in revised form
9 July 2018
Accepted 19 July 2018
Available online 9 August 2018

Keywords:
Relative sea level
Holocene
Hierarchical statistical modelling
Glacial-isostatic adjustment
Atlantic coast of Europe

A B S T R A C T

High-quality relative sea-level (RSL) data reveal spatial and temporal variations in crustal movements during the Holocene, which are used for many applications, ranging from calibrating models of earth rheology and ice sheet reconstructions to the development of coastal lowlands and human occupation. Here, we present a Holocene RSL database for the Atlantic coast of Europe (ACE) and estimate rates of RSL change from the ACE database using a spatio-temporal empirical hierarchical model. The database contains 214 index points, which locate the RSL position in space and time, and 126 limiting dates, which constrain RSL to above or below a certain elevation at a specific point in time. The temporal distribution extends from present to ~11.5 ka, with only 42 index points older than 7 ka. The spatial distribution spans 1700 km from French Flanders (France) to Algarve (Portugal), with more than half of the index points concentrated along the French coast.

The ACE database shows RSL was below present during the Holocene. Rates of RSL change were highest during the early Holocene, ranging between 6.8 ± 0.5 mm yr^{-1} in middle Portugal and 6.3 ± 0.8 mm yr^{-1} in southern France from 10 to 7 ka. Mid-to late-Holocene rates decreased over time with rates ranging between 0.9 ± 0.4 mm yr^{-1} in middle France and 0.1 ± 0.5 mm yr^{-1} in middle Portugal from 4 ka to present. Comparison of the RSL data to output from a glacial-isostatic adjustment model suggests that deglaciation of the British-Irish and Fennoscandian Ice Sheets dominates the large-scale variability captured by the ACE database, which reflects a decreasing influence of the collapsing British-Irish and Fennoscandian peripheral forebulge that migrated from the northeast to the northwest after ~4 ka.

1. Introduction

Modern sea-level rise associated with contemporary climate warming represents one of the most important challenges facing coastal communities (Church et al., 2013; Hinkel et al., 2015; Mengel et al., 2016; Chen et al., 2017; Horton et al., in press). The challenge from sea-level rise is not uniform, but instead reflects spatial variability in the rate of relative sea-level rise (Nicholls et al., 2014; Love et al., 2016). Local relative sea level (RSL: height of the sea surface with respect to the surface of the solid Earth) can differ considerably from the global mean value, because of vertical land motion and geoid change caused by a variety of processes, including the surface loading response to past glacial-isostatic adjustment (GIA) and contemporary land ice mass changes, tectonics, atmosphere-ocean dynamics that affect the height of the sea surface relative to the geoid, and local processes such as sediment compaction and tidal-range change (Milne et al., 2009; Kopp et al., 2015).

Spatial variability of past RSL changes is dominated by GIA (Milne et al., 2005). During the Last Glacial Maximum, large ice sheets covered high-latitude regions bordering the North Atlantic (Laurentide, Fennoscandian and British-Irish Ice Sheets), causing land subsidence beneath the ice sheet and uplift of the land surface/

* Corresponding author. Departamento de Estratigrafía y Paleontología, Universidad del País Vasco UPV/EHU, Bilbao, Spain.
E-mail address: ane.garcia@ehu.eus (A. García-Artola).

https://doi.org/10.1016/j.quascirev.2018.07.031

ocean floor in peripheral regions, the so-called "proglacial forebulge" (Peltier, 1996; Lambeck et al., 2014). During deglaciation, the viscoelastic response of the Earth reversed and regions beneath the ice sheets underwent isostatic uplift, while the forebulge collapsed, causing subsidence (Peltier, 1996, 2004; Mitrovica and Milne, 2002). Holocene RSL databases have been constructed from near- (beneath ice sheets), intermediate- (peripheral to ice sheets), and far-field (distal to ice sheets) regions in North America (Engelhart and Horton, 2012; Engelhart et al., 2015), the Caribbean (Milne and Peros, 2013; Khan et al., 2017), Europe (Lambeck et al., 1998; Brooks and Edwards, 2006; Vacchi et al., 2016), and elsewhere (Horton et al., 2005) that respond to these differing GIA signals (Khan et al., 2015). The Holocene databases have been constructed following the standardized methodology developed by the International Geological Correlation Projects (IGCP) 61, 200, 495, and 588 (e.g., Preuss, 1979; Tooley, 1982; Shennan and Horton, 2002; Hijma et al., 2015) and provide crucial constraints for parameters of Earth and ice components of GIA models (Milne and Peros, 2013; Roy and Peltier, 2015; Bradley et al., 2016).

In Europe, the RSL database from Great Britain and Ireland represents near- and intermediate-field locations mainly associated with the GIA response to the British-Irish Ice Sheet (Shennan and Horton, 2002; Brooks and Edwards, 2006; Bradley et al., 2011). Leorri et al. (2012a,b) compared RSL histories in locations (i.e., Brittany, France; Basque Country, Spain; Minho, Tagus Valley, and Algarve, Portugal) from the Atlantic coast of Europe (ACE) to the GIA model developed by Bradley et al. (2011). They identified a north-south GIA gradient that extends from northern France to the south of Portugal. However, Goslin et al. (2013, 2015) highlighted the unreliability of some of the data from the Brittany region used by Leorri et al. (2012a) to validate the GIA model predictions. Stéphan and Goslin (2014) reinterpreted the results from Leorri et al. (2012a) to develop a Holocene RSL database for the Atlantic coast of France, but they did not compare their data with output from a GIA model.

Here, we reinterpret previous compilations (Leorri et al., 2012a; Stéphan and Goslin, 2014) and incorporate new reconstructions to produce a standardized Holocene RSL database for the ACE. The goal of constructing the present database is to better understand the spatially-variable RSL history and influence of GIA along the ACE. Our database consists of 214 sea-level index points and 126 limiting data from northern France (51.1°N and 2.5°E) to southern Portugal (37°N and 8°W) (Fig. 1). We subdivide the database into 13 regions based on distance from the British-Irish and Fennoscandian Ice Sheets. We account for the influence of sediment compaction and explain sources of vertical and temporal uncertainty. We apply a spatio-temporal empirical hierarchical model (Kopp et al., 2016) to analyze the spatial variability and the rates of RSL change and compare the observations with predictions from the Bradley et al. (2016) GIA model.

2. Study area

The ACE database covers most of the French, northern Spain's, and the Portuguese coast (Fig. 1). France and Spain are considered to be tectonically stable on Holocene timescales (Boillot et al., 1979; Morzadec-Kerfourn, 1995; Chaumillon et al., 2010; Delgado et al., 2012), although some activity has been reported in various sites of France (Klingebiel and Gayet, 1995; Gandouin et al., 2007) and northwestern Spain (Alonso and Pagés, 2010). The Portuguese coast is known for neotectonic activity (de Groot and Granja, 1998; Terrinha, 1998; Dias, 2001) that has manifested as well-documented historical seismicity (Chester, 2001; Baptista et al., 2003; Besana-Ostman et al., 2012).

The climate of the ACE, following the Köppen climate classification, varies from temperate oceanic in France and northern Spain, temperate Mediterranean (with warm summers) in northwest Spain and the northern half of Portugal, and warm Mediterranean (with hot summers) in the southern half of Portugal. In northern France, mean annual temperature is ~10.6 °C and mean annual precipitation ranges from 711 to 1085 mm (Caen and Brest stations; Muhr, 2016). In middle to southern France, mean annual temperature ranges from 11.9 °C to 12.4 °C, and mean annual precipitation ranges from 789 to 905 mm (Nantes and Bordeaux stations; Muhr, 2016). In northern Spain, mean annual temperature ranges from 12.7 °C to 14.1 °C and mean annual precipitation ranges from 971 to 1581 mm (San Sebastian, Oviedo, and A Coruña stations; Muhr, 2016). In northwestern Spain and Portugal, mean annual temperature ranges from 13.4 °C to 14.8 °C and mean annual precipitation ranges from 1142 to 1952 mm (Vigo and Porto stations; Muhr, 2016). In mid-southern Portugal, mean annual temperature is ~17.1 °C and mean annual precipitation ranges from 522 to 679 mm (Lisbon and Faro stations; Muhr, 2016).

Great diurnal tidal range, from mean high water springs (MHWS) to mean low water springs (MLWS), along the ACE, varies from macrotidal in France (between 11.40 m during spring tides and 1.95 m during neap tides) to mesotidal regimes in northern Spain and Portugal (between 3.92 m during spring tides and 1.20 m during neap tides). Tidal datums for our study sites were obtained from the nearest tidal-reference station up to 72.2 km away (see column 77 in Appendix 1; extracted from SHOM (2016) for France, Puertos del Estado (2014) for Spain, and Admiralty Tide Tables (2015) for Portugal).

3. Material and methods

3.1. Relative sea-level (RSL) reconstruction

A sea-level index point estimates the position of RSL at a single point in space and time (Shennan and Horton, 2002). Where a suite of sea-level index points exists for a locality or region, they describe changes in RSL through time and can be used to estimate rates of RSL change (Engelhart et al., 2011). A sea-level index point is a datum that contains information about the geographical position, elevation, indicative meaning, and age of a sample. The methodology that is employed to produce valid sea-level index points is described in 'The Manual of Sea-level Research' (Shennan et al., 2015) and many other publications (e.g., Shennan, 1986; van de Plassche, 1986; Engelhart and Horton, 2012).

3.1.1. Vertical position of RSL

To produce a sea-level index point, the indicative meaning of a dated sample must be estimated (Shennan and Horton, 2002). The indicative meaning of a sample describes the relationship of the environment in which it accumulated relative to a contemporaneous reference tide level (van de Plassche, 1986). The indicative meaning varies according to the type of sea-level indicator and it is commonly expressed in terms of an indicative range and a reference water level (RWL) (Horton et al., 2000). The former is a vertical range within which the coastal sample may occur and the latter a water level to which the sample is related, for example, mean higher high water (MHHW), mean tide level (MTL), etc. (Shennan et al., 2015). To allow for sea-level trends to be inferred from multiple types of sea-level indicators and for comparisons to be made between different areas, each sample is related to its own reference tide level (Shennan, 1986).

Indicative meanings for the ACE database (Table 1) were estimated using published and unpublished data relating the distribution of modern salt-marsh, estuarine and lagoonal samples to elevation with respect to the tidal frame (Cearreta, 1998; Fatela

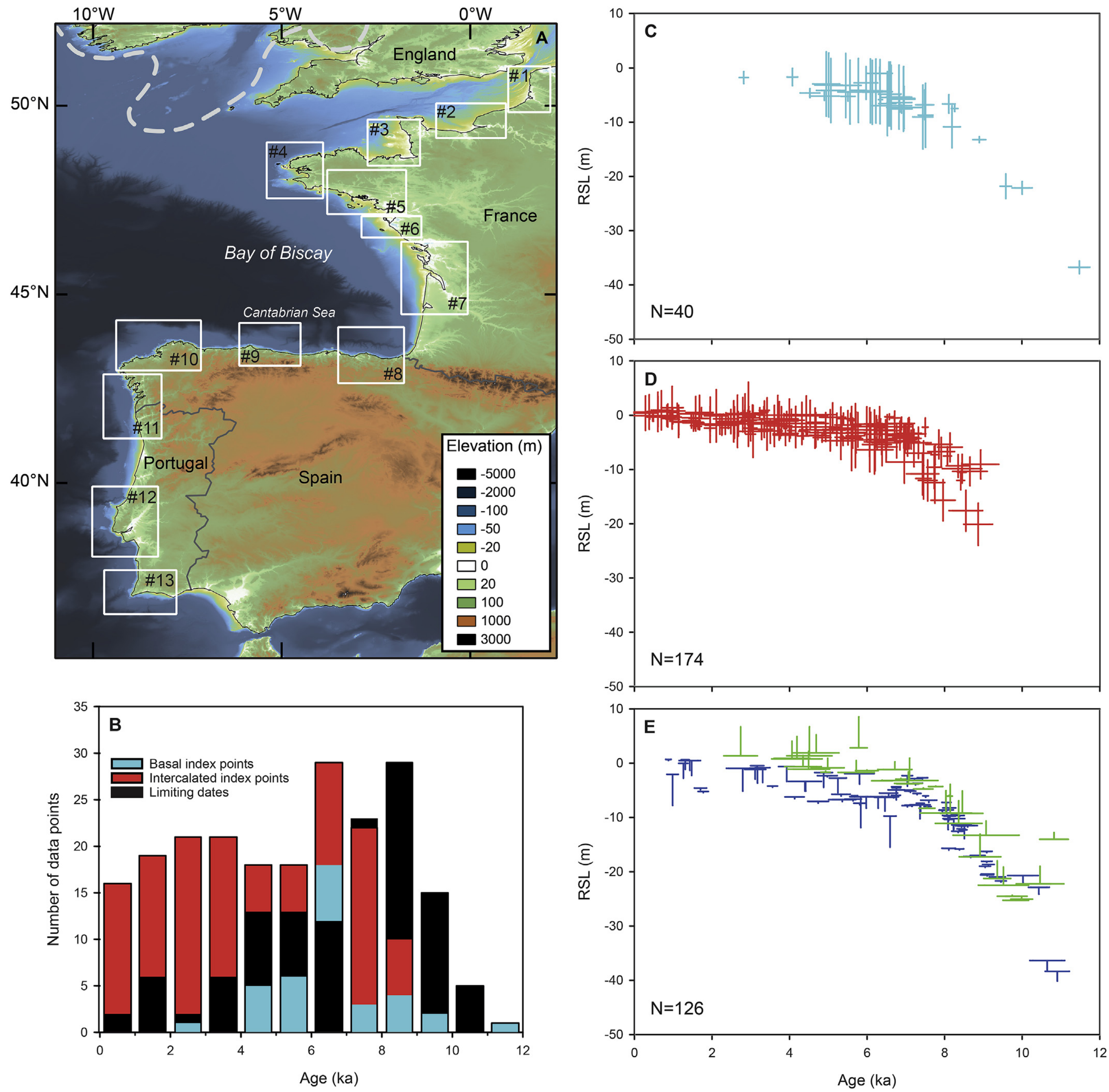

Fig. 1. Location map of the Atlantic coast of Europe database; dashed grey line represents the southern extent of British-Irish Ice Sheet during Last Glacial Maximum (Clark et al., 2012) (A). Number and types of data points in 1-ka time intervals (B). Temporal distribution of basal (C) and intercalated (D) index points and limiting dates (E).

et al., 2009; Stéphan et al., 2015a; Camacho et al., 2017). Within a salt marsh, it is usually possible to observe a clear vertical division of plants into high marsh and low marsh zones, which reflects the preferences and tolerances of halophytic species to the frequency and duration of tidal inundation (Kemp et al., 2010). The high to middle marsh environments in France and Spain, occurring broadly between highest astronomical tide (HAT) and mean high water (MHW), are generally covered by *Phragmites australis*, *Scirpus maritimus*, *Juncus maritimus, Halimione portulacoides*, and *Puccinellia maritima* vegetation (as well as *Plantago maritima* in France and *Elymus pycnanthus* in Spain); the middle to low marsh (between MHW and MTL) is represented by the halophytic plant species *Salicornia fragilis* and *Spartina alterniflora* in France and *Salicornia ramosissima and Spartina maritima* in Spain (Benito and Onaindia, 1991; Stéphan et al., 2015a). In southern Portugal, the high marsh is dominated by *Sarcocornia perennis* spp. *Alpine* and *Suaeda vera*, and the middle marsh by *H. portulacoides* and *Spartina densiflora*. The low marsh is dominated by *S. perennis* spp. *perennis* and *S. maritima,* as well as taxa found in the middle marsh (Camacho et al., 2017).

Similarly, studies of salt-marsh microfossils, such as foraminifera, diatoms, pollen, and ostracods, have shown that assemblages have characteristic preferences for particular elevations in the intertidal zone (Horton et al., 2006; Kemp et al., 2009;

Table 1
Definition of the indicative meanings used to develop the Atlantic coast of Europe database. HAT: highest astronomical tide. MHW: mean high water. MTL: mean tide level. MLW: mean low water.

Sample type	Evidence	Reference water level	Indicative range
Index Points			
High marsh environment	1. Foraminiferal assemblages dominated by high marsh taxa in an organic and/or minerogenic sediment (e.g., Cearreta et al., 2002; Stéphan et al., 2015a; García-Artola et al., 2015). 2. Reed peat identified from plant macroremains or pollen (e.g., Goslin et al., 2013).	(HAT + MHW)/2	HAT-MHW
Low marsh environment	3. Foraminiferal assemblages dominated by low marsh taxa in a minerogenic and/or organic sediment (e.g., Tastet et al., 2000; Cearreta et al., 2002).	(MHW + MTL)/2	MHW-MTL
Undifferentiated salt-marsh environment	4. Foraminiferal assemblages dominated by high and low marsh taxa in a minerogenic and/or organic sediment (e.g., Hernández Martín, 2013). 5. Pollen (with diatoms, dinoflagellates or ostracods) dominated by halophilous taxa in a minerogenic and/or organic sediment (e.g., Huault, 1980, 1985; Tastet et al., 2000; Clavé et al., 2001).	(HAT + MTL)/2	HAT-MTL
Open lagoon or shallow marine environment	6. Foraminifera, diatoms and ostracod assemblages dominated by marine and brackish littoral taxa or inner estuarine taxa (e.g., Trog et al., 2013, 2015). Articulated bivalves of intertidal taxa in life position (e.g., Teixeira et al., 2005).	−1 m	MTL to −2 m
Inner or semi-enclosed lagoon	7. Foraminifera, diatoms and ostracod assemblages dominated by brackish littoral taxa or inner estuarine taxa (e.g., Bao et al., 1999; Trog et al., 2015).	−0.5 m	MTL to −1 m
Undifferentiated intertidal environment	8. Intertidal muds with halophilous pollen species, marine shells and dinoflagellates (e.g., Joly, 2004; Joly and Visset, 2009).	(HAT + MLW)/2	HAT-MLW
Limiting Points			
Marine limiting	9. Calcareous foraminiferal assemblages and marine shells in a minerogenic sediment, as well as lagoonal sediments that do not meet the requirements to be classified as index points (e.g., Cearreta, 1998; Teixeira et al., 2005; Vis et al., 2008; Mrani-Alaoui and Anthony, 2011).	MTL	Below MTL
Freshwater limiting	10. Fluvial gravels without foraminifera or marine shells (e.g., Schneider et al., 2010; Cearreta and Monge-Ganuzas, 2013). 11. Pollen assemblages dominated by freshwater taxa in an organic sediment (e.g., Tastet et al., 2000). 12. Freshwater shells in an organic sediment (e.g., Gabet, 1973).	MTL	Above MTL

Schneider et al., 2010). Similar to Engelhart and Horton (2012), we inferred that samples identified to be from salt-marsh origin formed between HAT and MTL. If preserved plant macrofossils (e.g., reed fragments) or microfossils (e.g., foraminifera) suggested a high marsh environment, an indicative range of HAT to MHW was assigned to the sample. For low marsh environments, the indicative range applied was MHW to MTL. Pollen assemblages were used to identify an undifferentiated salt-marsh environment when halophilous taxa were found in organic sediment.

Some index points from Portugal were derived from lagoonal/shallow marine samples that were classified as either open or semi-enclosed environments based on the presence of certain articulate bivalve, ostracod, and foraminifera taxa. We corrected the Leorri et al. (2012a) data for southern Portugal (Teixeira et al., 2005) to incorporate the indicative meaning. We applied the same indicative meanings suggested by Vacchi et al. (2016) for these lagoonal samples of MTL to −2 m (open) and MTL to −1 m (enclosed), except for samples that contained the articulated bivalves *Cerastoderma glaucum* and *Loripes lacteus*. According to Teixeira et al. (2005) these species are infra-littoral taxa and can live > 2 m below MTL in the Algarve region, so they were considered as marine limiting dates. Finally, we adopted a broad indicative meaning for those samples with a mixture of marine and brackish water indicators that we classified as an undifferentiated intertidal environment, between HAT and mean low water (MLW).

Where biostratigraphic data indicated formation and deposition in a freshwater or marine environment, the sample was classified as a limiting date. Reconstructed RSL must fall below freshwater limiting dates and above marine limiting dates. Although limiting dates cannot constrain the precise position of past sea level, they are extremely important in understanding and interpreting sea-level changes, as well as constraining GIA models (e.g., Shennan and Horton, 2002; Engelhart and Horton, 2012).

Freshwater limiting dates form at an elevation above the tidal influence, commonly above HAT; however, these depositional environments may possibly be linked to rising groundwater, and therefore we used a RWL of above MTL (Jelgersma, 1961; Shennan et al., 2000; Engelhart and Horton, 2012). Freshwater limiting dates from the ACE were derived from organic sediment samples with freshwater indicators (e.g., Gabet, 1973; Tastet et al., 2000) or fluvial sediments where marine indicators were absent (e.g., Cearreta and Monge-Ganuzas, 2013).

Marine limiting dates form below MTL. The majority of marine limiting dates from the ACE were retrieved from estuarine muddy or sandy environments with a very low organic matter content (i.e., tidal flat). Previous regional RSL reconstructions (i.e., Leorri et al., 2012a; Stéphan and Goslin, 2014) had interpreted tidal flat sediments as index points, but we plotted them as marine limiting dates because it is often difficult to determine the lower limit of these environments. Where possible, we used dates from marine shells recovered in living position (e.g., Teixeira et al., 2005). We eliminated those samples recovered from depositional environments highly prone to remobilization (e.g., channel bottom sediments).

The mean estimate of RSL for each index point was calculated as:

$$RSL_i = E_i - RWL_i \quad (1)$$

where E_i and RWL_i are the elevation and reference water level of sample *i*, expressed relative to the same tidal datum (e.g., MTL; Shennan and Horton, 2002). For a modern (surface) sample, the terms E_i and RWL_i are equal, thus RSL will be zero. All index points in the database are expressed in relation to this value, where negative values indicate RSL below present.

Elevation within the ACE was commonly established by referring the samples to an orthometric datum by means of a total station or a GPS. Sometimes this information was not available, and we estimated the elevation based on the local vegetation referenced to mean sea level (MSL), measured at the nearest tidal-reference station.

3.1.2. Sources of uncertainty for the vertical position of RSL

The uncertainty for the vertical position of RSL takes into account many sources of uncertainty; many of which can be quantified following Shennan and Horton (2002). Apart from the uncertainty associated with the indicative meaning (i.e., the indicative range), there are a series of additional uncertainties related to the determination of the depth of a sample in the core and the elevation of the core. To determine the uncertainty associated with the sample depth, we have taken into account the sample thickness (measured or estimated), the sampling uncertainty, the compaction associated with the sampling method, and the angle of the borehole that decreases with depth (non-vertical drilling uncertainty). To determine the uncertainty associated with calculating the elevation of a sample, we considered the tidal range and water depth for samples obtained offshore, the uncertainty of the total station, GPS or Real Time Kinematic (RTK), and the benchmark for high-precision surveying. When these uncertainties were not specified in the original publications, we used the recommended values by Hijma et al. (2015) shown in Table 2. We assigned an uncertainty of half the tidal range for samples where the orthometric elevation was reported but the methodology was unknown (e.g., Frouin et al., 2009; Gandouin et al., 2009). For elevations estimated from the distribution of local vegetation, we adopted an uncertainty of half the vertical distribution of the depositional environment (e.g., undifferentiated salt marsh).

There are two sources of uncertainty that we did not quantify: tidal range variation during the Holocene and sediment compaction. First, if the tidal range has not remained constant through the Holocene, sea-level index points based upon tide level indicators will differ from the 'true' sea-level position (Horton et al., 2013). For example, if the tidal range was amplified in the past, the elevation of the RWL of a salt-marsh indicator would have been greater and the true sea-level position lower (Horton et al., 2013; Hill, 2016). There have been notable attempts to characterize tidal range change for ACE (Goslin et al., 2015; Ward et al., 2016). Goslin et al. (2015) concluded paleotidal changes were minor since 8 ka, and especially after 6 ka, when tidal ranges reached their current values as sea-level was close to the current position. Ward et al. (2016) show their model is sensitive to choice of the GIA model (rather than the hydrodynamic model). Here, we are constructing the most complete Holocene RSL database for ACE that will be used in the future to improve GIA modelling. Therefore, although the tidal range changes are suggested to be minor, the quantitative value is unknown.

The second form of uncertainty for the vertical position of RSL, which we do not quantify is post-depositional lowering due to compaction of underlying sediment. This unidirectional process causes the underestimation of the RSL position. However, we qualitatively evaluate the possible influence of compaction by dividing the sea-level index points into basal and intercalated (Horton and Shennan, 2009). Basal samples are derived from sediments lying directly above an incompressible substrate, while the intercalated samples are susceptible to compaction because they are located between non-basal clastic sediments (Jelgersma, 1961). In addition, we have only considered freshwater limiting dates coming from basal sediments to avoid high-limiting constraints affected by compaction plotting below sea-level index points.

3.1.3. *Age and uncertainty of RSL*

All sea-level index points and limiting dates were radiocarbon dated (Accelerator Mass Spectrometry, AMS or radiometric) and expressed as calibrated years before present (BP, measured with respect to 1950 CE). All dates obtained prior to the mid-1980s were corrected for isotopic fractionation following Stuiver et al. (2017). When $\delta^{13}C$ values were not reported, we assigned standard values (−27‰ for terrestrial and 0‰ for marine samples). To account for the possibility of multiple sources of carbon supply in bulk sediment samples (e.g., freshwater, salt-marsh, or tidal flat bulk organic/minerogenic sediment), we added an additional uncertainty of ±100 years (Hu, 2010).

We calibrated all index points and limiting dates using CALIB 7.1 (Stuiver et al., 2017) with a 2σ confidence interval. Terrestrial samples (e.g., wood fragment, freshwater and salt-marsh organic/minerogenic sediment) were calibrated using the IntCal13 calibration curve (Reimer et al., 2013). Marine samples (e.g., bivalve shells and calcareous foraminifera) were calibrated using the Marine 13 calibration curve (Reimer et al., 2013). For samples dated using *Hydrobia* shells, we applied the mixed Marine and Northern Hemisphere Atmosphere curve (Reimer et al., 2013) for calibration following Billeaud (2007). For marine samples, we used the

Table 2
Standardized vertical uncertainties adopted for the construction of the Atlantic coast of Europe database.

Sources of uncertainty	Description
Uncertainties related to the indicative meaning of a sample	
Indicative range uncertainty	± indicative range/2
Uncertainties related to the determination of the depth of a sample in a core	
Sample thickness uncertainty[a]	± sample thickness/2
Sampling uncertainty	±0.01 m
Core shortening/stretching uncertainty	±0.15 m for rotary coring and vibracoring ±0.05 m for hand coring ±0.01 m for a Russian sampler
Non-vertical drilling uncertainty	0.02 m/m depth
Uncertainties related to the determination of the elevation of a core	
Offshore sample collection	
Tidal uncertainty	± tidal range/2
Water depth uncertainty	±0.5 m
High-precision surveying methods	
Total station uncertainty	±0.01 m
GPS or RTK uncertainty	±0.1 m
Benchmark uncertainty	±0.1 m
Unknown methods	
Tidal uncertainty	± tidal range/2
Estimation from vegetation zone	
Undifferentiated salt-marsh vertical distribution uncertainty	± (HAT-MTL)/2
High marsh vertical distribution uncertainty	± (HAT-MHW)/2

[a] When the sample thickness was not originally reported it was estimated from the dating method (0.1 m for AMS and 0.5 m for radiometric dating).

following average (spatial and temporal) local marine reservoir corrections (ΔR): -7 ± 50 years (Tisnérat-Laborde et al., 2010) for the French Atlantic coast (regions #1, #3, #6, and #7); -105 ± 21 years (Monge Soares et al., 2016) for the Cantabrian Sea (region #8); -192 ± 24 years (Monge Soares and Dias, 2007) for the northern Galician coast (region #10); 95 ± 15 years (Monge Soares and Dias, 2006) for the central Portuguese coast (region #12); and 69 ± 17 years (Martins and Monge Soares, 2013) for the southwest Portuguese coast (region #13).

3.1.4. Example of a sea-level index point from northern Spain

An intercalated sea-level index point was recovered from the Anbeko salt marsh that has recently been reclaimed for cattle grazing and is located in the lower-middle Urdaibai estuary (northern Spain) (Fig. 2). The litho- and bio-stratigraphy of Anbeko salt marsh is characterized by 3.3 m of gravels without foraminifera at the base of the core which was overlain by 8.1 m of mud with bioclasts and then 9.6 m of sand with bioclasts dominated by calcareous foraminifera from an estuarine environment. Above the sand were 6.9 m of sandy mud and mud with plant remains with agglutinated foraminifera, suggesting a salt-marsh environment (Cearreta and Monge-Ganuzas, 2013).

We extracted a 4.80 m sediment core (AN2) from Anbeko salt marsh using a rotary drill. We measured the surface elevation of the core using a GPS-RTK (±0.02 m leveling uncertainty), which was tied into a benchmark (±0.10 m estimated benchmark uncertainty) to which the tidal datum is referenced. The core surface elevation was 1.81 ± 0.12 m NMMA (or MSL in Alicante, the Spanish orthometric datum defined in the Mediterranean coast) or 1.50 ± 0.12 m MSL at the nearest Bilbao tide gauge.

A small halophytic plant remain within the muddy sediment was selected at a depth of 2.72 m (−1.22 m MSL) for AMS dating. The AMS dated plant remain (Beta-463064) yielded a calibrated age of 4421 to 4248 cal BP, which represents the horizontal 2σ range of the sea-level index point.

The foraminiferal assemblage at this depth was dominated by the agglutinated species *Entzia macrescens* (90%), *Trochammina inflata* (6%), and *Arenoparrella mexicana* (4%) that are typical of a high marsh environment. The RWL of the sample was calculated as the midpoint between HAT and MHW, and the indicative range uncertainty as half the elevation difference between HAT and MHW. The elevation of HAT and MHW is 2.39 m MSL and 1.36 m MSL, respectively, at the nearest tide gauge (Bilbao). Therefore, the sample's RWL is 1.87 m MSL and the indicative range is 1.03 m, with an associated indicative range uncertainty of ±0.52 m. We calculated the total uncertainty for this sample from the following uncertainty terms: sample thickness uncertainty of ±0.01 m; non-vertical drilling uncertainty of ±0.01 m; core shortening uncertainty of ±0.15 m; and a standard sampling uncertainty of ±0.01 m.

The calculation of RSL and its uncertainty for this index point was:

$$\text{RSL} = -1.22\ \text{m}_{\text{elevation}} - 1.87\ \text{m}_{\text{RWL}} = -3.09\ \text{m}$$

$$\text{RSL uncertainty} = \pm[(0.52\ \text{m})^2_{\text{indicative range}} + (0.12\ \text{m})^2_{\text{elevation}} + (0.01\ \text{m})^2_{\text{sample thickness}} + (0.01\ \text{m})^2_{\text{angle borehole}} + (0.15\ \text{m})^2_{\text{coring method}} + (0.01\ \text{m})^2_{\text{sampling}}]^{1/2} = 0.55\ \text{m}$$

The minerogenic nature of the sediment undelying the index point minimizes the influence of compaction (Brain et al., 2011).

3.2. Statistical analysis

We fit the RSL index points with a spatio-temporal empirical hierarchical model (Cressie and Wikle, 2011; Kopp et al., 2016; Ashe et al., in review), implemented using the CESL-STEHM-GP code base for MATLAB (Kopp, 2016). A hierarchical model separately distinguishes between process-level variability in the underlying spatio-temporal RSL field, which reflects the different mechanisms that cause RSL to vary over space and time, and data-level noise, reflecting geochronological uncertainty, vertical measurement uncertainty, and the indicative range. Prior expectations about scales of variability are described by hyperparameters. In an empirical model, these hyperparameters are optimized to maximize the likelihood of the model given the observations. Once the parameters are optimized, the resulting prior probability distribution is conditioned upon the observations to generate a posterior estimate of the spatio-temporal RSL field and its components. Rates are derived from the posterior estimate of this field through a linear transformation.

As applied here, the process level decomposes the spatio-temporal field of RSL change, which we denote $f(\boldsymbol{x},t)$, into four components, representing (1) a slowly changing signal common to the region of study, $g(t)$, (2) a long-wavelength regional signal, $r(\boldsymbol{x},t)$, (3) a short-wavelength regional signal, $s(\boldsymbol{x},t)$, and (4) high-frequency, localized variability, represented as white noise, $w(\boldsymbol{x},t)$:

$$f(\boldsymbol{x},t) = g(t) + r(\boldsymbol{x},t) + s(\boldsymbol{x},t) + w(\boldsymbol{x},t) \quad (2)$$

Here, $\boldsymbol{x}$ represents geographic location and t represents time.

Each of the four components on the right-hand side of equation [2] is characterized by a Gaussian-process prior, which expresses expectations in the absence of observations about how the component should behave (Rasmussen and Williams, 2006). A Gaussian-process prior is characterized by a mean function, which we assume is zero at all points in space and time, and a covariance function, which encodes expectations regarding how strongly correlated different points in space and time are with one another. Here, we use spatially and temporally separable Matérn covariance functions. The spatial component is a Matérn-1/2 function, which allows for the possibility that RSL exhibits abrupt changes in spatial gradient and is not spatially differentiable. The temporal component is a Matérn-3/2 function, which yields time series that are once differentiable (allowing for abrupt changes in acceleration but not in rate); this differentiability is a requirement for the approach we use to handle geochronological uncertainty, as discussed below.

The optimized hyperparameters for these components are shown in Table 3. For example, the spatially uniform term $g(t)$ is a priori expected to exhibit variability with a standard deviation of ±78.2 m and a decorrelation timescale of about 37 ka; the long-wavelength regional signal $r(\boldsymbol{x},t)$ is expected to exhibit variability on the scale of ±2.6 m, with a decorrelation timescale of about 6.5 ka and a decorrelation length scale of about 13.0°. The optimized hyperparameters indicate that the more local terms [$s(\boldsymbol{x},t)$ and $w(\boldsymbol{x},t)$] contribute minimally to the overall signal [see Table 3: prior standard deviations of ±3 cm for $s(\boldsymbol{x},t)$ and ±0.2 mm for $w(\boldsymbol{x},t)$]; almost all deviations from the spatially uniform signal and the longer-wavelength regional signal can be explained by individual sample uncertainty at the data level.

As applied here, the data level represents each individual RSL estimate y_i and age observation $\hat{t}_i$ as a noisy corruption of true RSL and true age, $f(\mathbf{x},t_i)$ and t_i:

$$y_i = f(\boldsymbol{x}_i, t_i) + \varepsilon_i \quad (3)$$

$$\hat{t}_i = t_i + \delta_i \quad (4)$$

Here, i indexes the individual observations, ε_i represents the vertical measurement and indicative range error associated with observation i, and δ_i represents the geochronological error

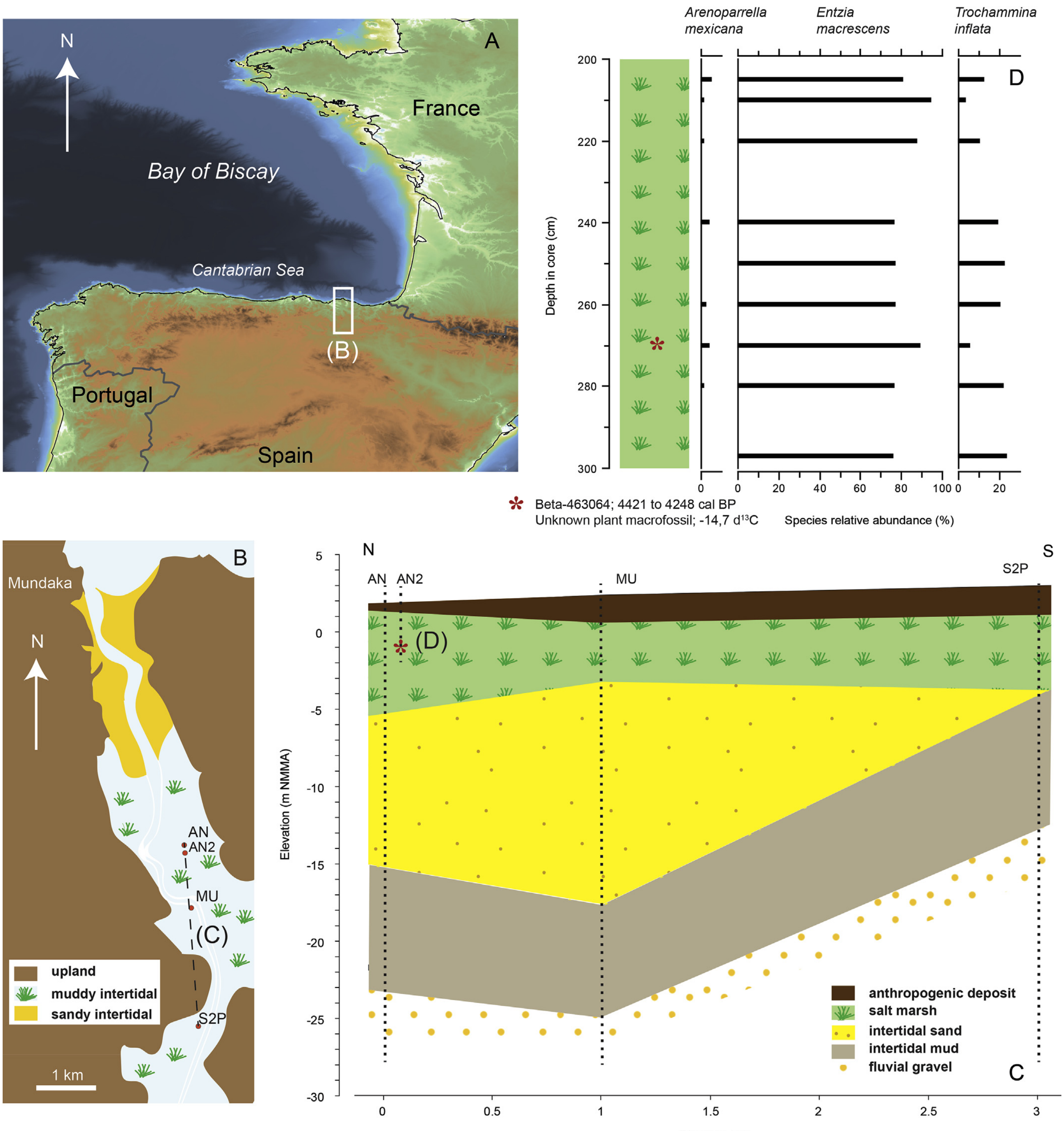

Fig. 2. Example site location in Basque Country (region #8) (A). Urdaibai estuary map with the location of analyzed cores for stratigraphical purposes (B). Stratigraphic section of the middle Urdaibai estuary (C). Foraminiferal diagram for the sea-level index point from core AN2 (D).

associated with measurement *i*. Geochronological uncertainties are approximated using the Noisy-Input Gaussian Process approximation (McHutchon and Rasmussen, 2011), which uses the slope of a time-series at a point to translate an error in the independent variable (here, age) into a comparable error in the dependent variable (here, RSL). Standard deviations for the vertical and temporal uncertainty terms in equations [3] and [4] are defined in the database.

4. Holocene relative sea-level records of the Atlantic coast of Europe

4.1. French Flanders and Picardy coastal plain (region #1)

The RSL history consists of 16 index points, eight marine limiting dates, and eight freshwater limiting dates (Fig. 3). In the early Holocene, between ~10.4 and ~9.3 ka freshwater limiting dates

Table 3
Optimized hyperparameters.

prior standard deviation of $g(t)$	78.2 m
prior timescale of $g(t)$	37.3 ka
prior standard deviation of $r(\boldsymbol{x},t)$	2.6 m
prior timescale of $r(\boldsymbol{x},t)$ and $s(\boldsymbol{x},t)$	6.5 ka
prior length scale of $r(\boldsymbol{x},t)$	13.0°
prior standard deviation of $s(\boldsymbol{x},t)$	0.03 m
prior length scale of $s(\boldsymbol{x},t)$	1.0°
prior standard deviation of $w(\boldsymbol{x},t)$	0.2 mm

constrain RSL to below -21.1 ± 3.3 m. The oldest index point places RSL at -17.7 ± 3.8 m at ~8.6 ka. Then, RSL rose to -11.8 ± 3.8 m at ~7.5 ka at a rate of 5.7 ± 1.2 mm yr^{-1}. A freshwater limiting date constrains RSL to below -3.1 ± 4.2 m at ~7.1 ka. Younger index points show RSL rose from -3.3 ± 3.8 m at ~5.7 ka to -1.8 ± 3.3 m at ~2 ka at a rate of 1.2 ± 0.5 mm yr^{-1}. Two marine limiting dates indicate that RSL was above 0.1 ± 2.7 m between ~1.5 and ~1.2 ka.

4.2. Seine estuary and coast of Calvados (region #2)

The RSL record contains 20 index points and one freshwater limiting date (Fig. 3). The limiting date constrains RSL to below -22.3 ± 3.4 m at ~9.5 ka. The oldest index point places RSL at -20.2 ± 3.9 m at ~8.9 ka. RSL was at -10.8 ± 3.9 m at ~8.2 ka, and then it rose to -7.2 ± 3.9 m at ~6.9 ka at a rate of 4.3 ± 1.0 mm yr^{-1}

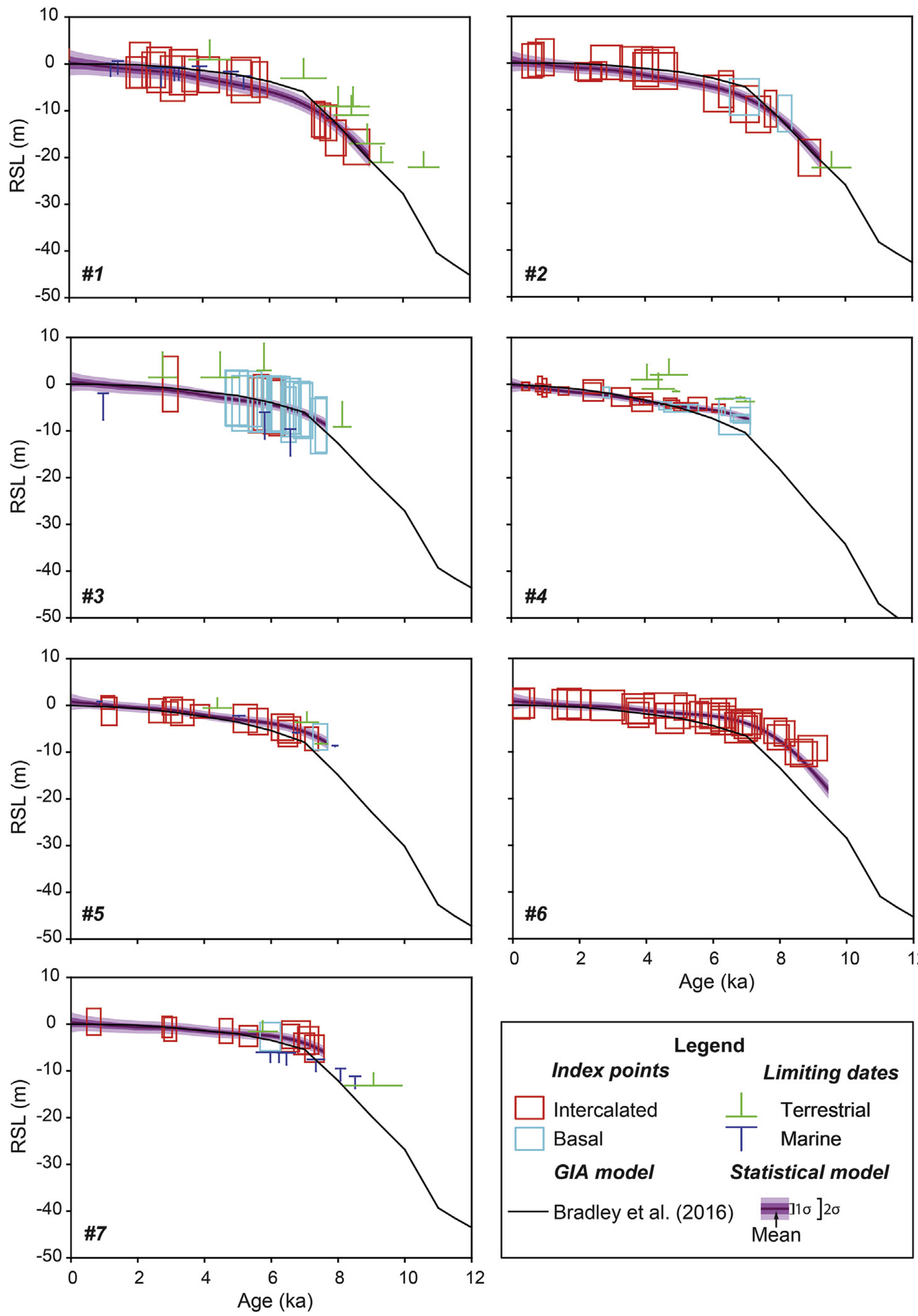

Fig. 3. RSL observations compared to GIA and spatio-temporal statistical model predictions for different coastal regions of France.

and to −6.5 ± 3.9 m at ~6.2 ka at a rate of 2.3 ± 0.8 mm yr^{-1}. RSL remained relatively stable during the late Holocene, reaching −0.2 ± 3.6 m at ~4.4 ka, although four index points suggest RSL was at ~ -2.0 ± 1.8 m between ~2.6 and ~2.2 ka.

4.3. Normano-Breton gulf and north Brittany (region #3)

The RSL record is based on 24 index points, three marine limiting dates, and four freshwater limiting dates (Fig. 3). The oldest freshwater limiting date indicates RSL was below −9.1 ± 5.4 m at ~8.1 ka. Index points show RSL rose from −8.7 ± 5.9 m at ~7.5 ka to −5.7 ± 5.9 m at ~6.9 ka at a rate of 3.4 ± 1.1 mm yr^{-1}, and to −2.9 ± 5.9 m at ~5 ka at a rate of 1.5 ± 0.5 mm yr^{-1}. During the late Holocene, data are scarce, and a single index point places RSL at 0.0 ± 5.9 m at ~3 ka. Finally, a marine limiting date indicates RSL was above −1.9 ± 5.7 m at ~1 ka.

4.4. West Brittany (region #4)

The West Brittany RSL record is composed of 28 index points and seven freshwater limiting dates (Fig. 3). The oldest index point locates RSL at −7.5 ± 0.8 m at ~6.9 ka. A series of index points show RSL rose relatively steadily to −0.4 ± 0.8 m at ~0.5 ka at a rate of 1.0 ± 0.2 mm yr^{-1}.

4.5. South Brittany (region #5)

The RSL record from South Brittany contains 14 index points, four marine limiting dates, and three freshwater limiting dates (Fig. 3). A marine limiting date suggests RSL was above −8.6 ± 0.2 m at ~7.9 ka. The oldest index point places RSL at −6.7 ± 2.8 m at ~7.5 ka. RSL rose from −5.2 ± 2.8 m at ~6.5 ka to −2.8 ± 3.0 m at ~5.2 ka at a rate of 1.0 ± 0.5 mm yr^{-1}. A freshwater limiting date constrains RSL to below −0.5 ± 2.1 m at ~4.3 ka. During the late Holocene, RSL remained relatively stable at −1.2 ± 1.4 to −1.3 ± 3.0 m between ~3.9 and ~1.2 ka.

4.6. Coast of Vendée (region #6)

The RSL record is derived from 32 index points (Fig. 3). The oldest index point in the early Holocene places RSL at −9.2 ± 2.7 m at ~8.9 ka. However, the next two index points locate RSL at ~−10 m at ~8.6 ka. RSL rose until ~7.9 ka at a rate of 6.7 ± 1.2 mm yr^{-1}, when it reached −5.5 ± 2.7 m. Then, RSL evolved from −5.0 ± 2.7 m at ~7.1 ka to the modern position at ~5.1 ka at a rate of 1.1 ± 0.4 mm yr^{-1}. Even though the general trend of the late Holocene RSL record shows an average position close to modern, there are 3 index points at ~4.9, ~4.7, and ~3.7 ka that suggest RSL was between −2.1 ± 2.7 and −2.8 ± 3.2 m.

4.7. Coast of charentes (region #7)

The RSL record is made of 11 index points, six marine limiting dates, and two freshwater limiting dates (Fig. 3). The oldest freshwater limiting date constrains RSL to below −13.1 ± 2.6 m at ~9 ka. Two marine limiting dates place RSL above −11.1 ± 2.6 m at ~8.5 ka and above −9.5 ± 2.6 m at ~8.1 ka. The oldest index point indicates RSL was at −5.2 ± 2.9 m at ~7.3 ka. RSL rose to −3.5 ± 2.9 m at ~7.1 ka. Then, RSL evolved from −3.0 ± 2.9 m at ~6.5 ka to −1.5 ± 2.6 m at ~4.7 ka at a rate of 0.7 ± 0.5 mm yr^{-1}. During the late Holocene RSL was at ~−1.0 ± 2.5 m at ~2.9 ka and at 0.5 ± 2.8 m at ~0.6 ka.

4.8. Basque Country (region #8)

The Basque Country RSL record consists of 12 index points, 47 marine limiting dates, and three freshwater limiting dates (Fig. 4). The database includes two index points from the Urdaibai estuary that were previously located in the Bilbao estuary in Leorri et al. (2012a). The RSL record from the early and mid-Holocene is derived from freshwater and marine limiting dates. Even though dates from shells recovered from the eastern Cantabrian coast have sometimes shown signs of reworking because of the high-energy coastal activity (Alonso and Pagés, 2000; Cearreta and Murray, 2000), the dates included in this database did not show inversions and were used to constrain RSL. Three freshwater limiting dates constrain RSL to below ~−25 m at ~9.8 ka. A series of marine limiting dates show RSL rose from above −21.6 m at ~9.4 ka to above −8.5 m at ~8 ka. Marine limiting dates indicate RSL evolved from above −5.9 m at ~7.5 ka to above −4.2 m at ~6.7 ka. There is a lack of data between ~6.7 and ~5.8 ka. Two marine limiting dates indicate RSL was above ~−5.8 m between ~5.7 and ~5.3 ka. The oldest index point places RSL at −3.3 ± 0.5 m at ~4.9 ka. RSL continued to rise at a rate of 0.4 ± 0.3 mm yr^{-1} during the late Holocene until ~1.6 ka, when it reached −2.1 ± 0.5 m.

4.9. Asturias (region #9)

The RSL record includes six index points and three marine limiting dates (Fig. 4). The oldest limiting date indicates RSL was above −10.1 m at ~8.2 ka. The oldest index point shows RSL was located at 7.1 ± 2.3 m at ~7.5 ka. Five younger index points indicate RSL rose from −5.5 ± 2.3 m at ~6.1 ka to −1.4 ± 2.3 m at ~1.2 ka at a rate of 0.6 ± 0.3 mm yr^{-1}.

4.10. Galicia (region #10)

The RSL record for Galicia is composed of five index points, eight marine limiting dates, and one freshwater limiting date (Fig. 4). Two marine limiting dates constrain RSL to above −38.2 m at ~10.9 ka and −36.2 m at ~10.6 ka. An early Holocene index point suggests RSL was at −21.7 ± 2.3 m at ~9.6 ka. RSL rose from −9.5 ± 2.1 m at ~8.4 ka to −4.1 ± 2.1 m at ~7 ka at a rate of 4.7 ± 0.8 mm yr^{-1}. During the late Holocene, one freshwater and three marine limiting dates constrain RSL to below −0.7 ± 1.8 m at ~5 ka and to above −3.2 ± 1.8 m at ~4.4 ka and −1.0 m at ~3.1 ka. Younger index points show RSL rose from −1.8 ± 2.1 m at ~2 ka to −0.2 ± 2.1 m at ~0.9 ka at a rate of 0.6 ± 0.7 mm yr^{-1}.

4.11. Southern Galicia and north of Portugal (region #11)

The RSL record contains eight index points, four marine limiting dates, and four freshwater limiting dates (Fig. 4). The early and mid-Holocene record is constrained only by marine and freshwater limiting dates. Marine limiting dates suggest RSL was above −22.7 ± 1.3 m at ~10.4 ka, −20.6 ± 1.3 m at ~10 ka, −6.7 ± 0.4 m at ~7.6 ka, and −5.4 m ± 0.4 at ~6.5 ka. Freshwater limiting dates suggest RSL was below −13.9 ± 1.3 m at ~10.8 ka, −4.2 ± 0.1 m at ~7.8 ka, −1.0 ± 1.4 m at ~6.7 ka, and −1.2 m ± 0.1 at ~6 ka. Late Holocene index points demonstrate RSL remained close to present, from −1.6 ± 1.1 m at ~2.4 ka to −0.2 ± 0.6 m at ~0.4 ka.

4.12. Lisbon and Tagus Valley (region #12)

The RSL history is constrained by 17 index points and four marine limiting dates (Fig. 4). The oldest index point indicates RSL was located at −36.7 ± 1.2 m at ~11.5 ka. RSL then rose to −2.4 ± 1.7 m at

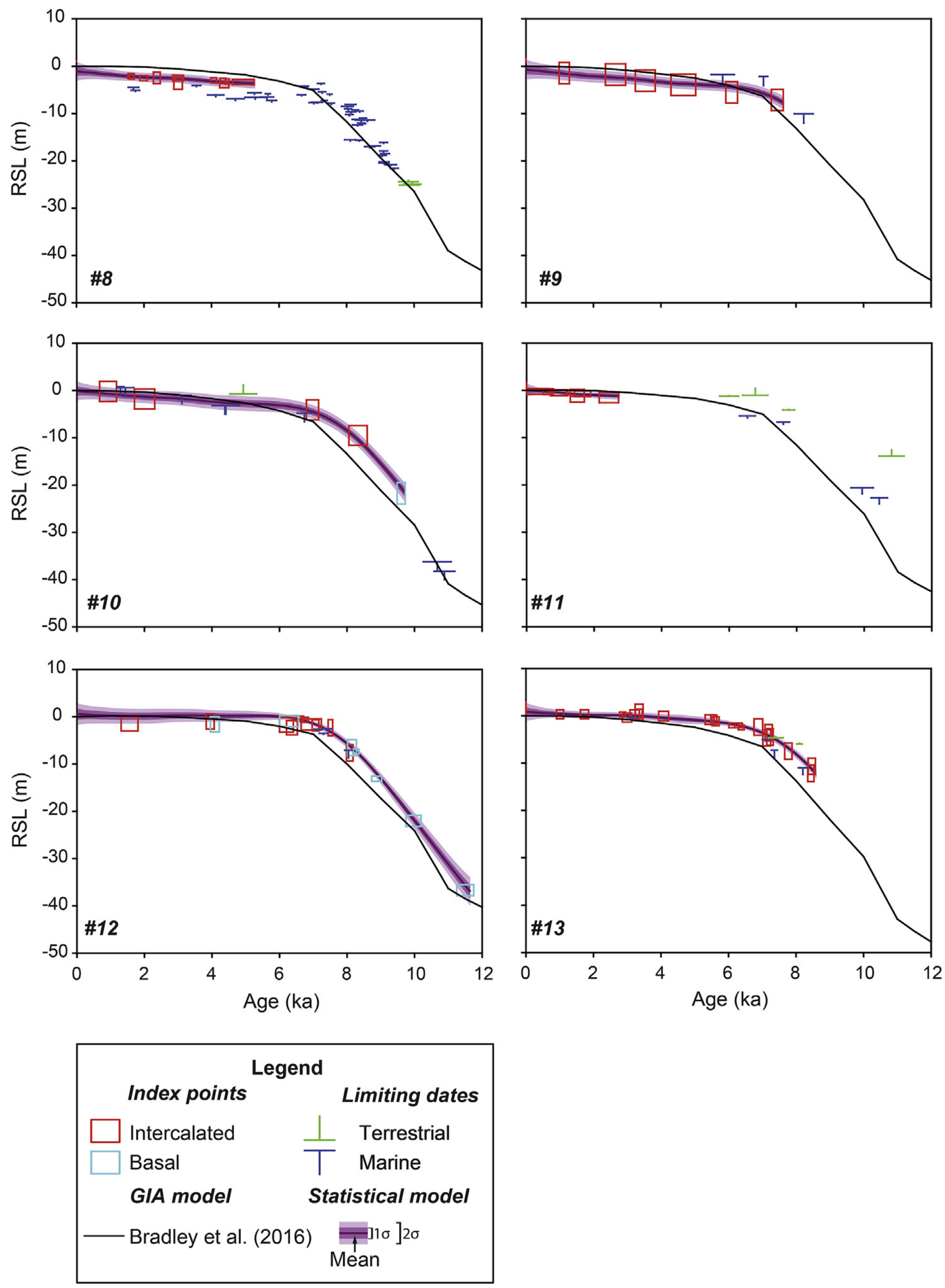

Fig. 4. RSL observations compared to GIA and spatio-temporal statistical model predictions for different coastal regions of Spain and Portugal.

~7.5 ka at a rate of 8.1 ± 0.7 mm yr^{-1} and to −1.6 ± 1.2 m at ~6.9 ka at a rate of 3.4 ± 1.0 mm yr^{-1}. A younger index point places RSL at −0.9 ± 1.2 m at ~6.3 ka. Index points indicate RSL rose from −1.6 ± 1.6 m at ~4.1 ka to −1.5 ± 1.5 m at ~1.5 ka at a rate of 0.0 ± 0.5 mm yr^{-1}.

4.13. Algarve (region #13)

The Algarve RSL record is derived from 21 index points, four marine limiting dates, and two freshwater limiting dates (Fig. 4). The oldest index point constrains RSL to −10.7 ± 1.7 m at ~8.5 ka. RSL rose to −3.6 ± 1.7 m at ~7.2 ka at a rate of 5.3 ± 0.6 mm yr^{-1}. Later, a series of index points indicate RSL rose from −2.5 ± 0.5 m at ~6.4 ka to 0.4 ± 0.9 m at ~1 ka at a rate of 0.5 ± 0.2 mm yr^{-1}.

5. Discussion

5.1. RSL reconstructions from the Atlantic coast of Europe

The Holocene RSL database for the ACE is made up of 214 index points and 126 limiting dates extracted from estuaries, coastal lagoons and salt marshes (Fig. 1). Most RSL reconstructions are derived from intercalated index points from salt-marsh and occasionally lagoonal sediments (regions #10–13) that extend back to ~11.5 ka. Only 40 basal index points are distributed between ~7 and ~5 ka. The general lack of basal data from the early Holocene has also been noted in other RSL databases such as the Mediterranean (Vacchi et al., 2016). Data are limited during the early Holocene because of restricted peat formation and preservation during periods of rapid RSL rise, as well as the difficulty in retrieving these coastal sediments, which occur mainly offshore (Brooks and Edwards, 2006; Törnqvist and Hijma, 2012). When the rate of marine transgression slowed at ~7 ka, the modern coastline and estuaries formed (Teixeira et al., 2005; Vis et al., 2008; Stéphan and Goslin, 2014), with basal peats occupying the base of the coastal sequences. Subsequently, the estuaries of the ACE infilled with tidal flat and salt-marsh sediments deposited mainly during the mid- and late Holocene (Boski et al., 2002; Vis and Kasse, 2009; Chaumillon et al., 2010; Fenies et al., 2010; Menier et al., 2010). The stabilization of RSL in the mid to late Holocene is reflected by the formation of coastal barriers, due to sediment transport along the coastline, and development of lagoons in low-lying coastal areas (Dias et al., 2000; Cearreta et al., 2003; Freitas et al., 2003; Naughton et al., 2007; Lespez et al., 2010; Stéphan and Laforge, 2013; Stéphan et al., 2015a,b).

Subdivision of index points within the ACE into basal and intercalated categories provides an initial assessment of the influence of compaction (e.g., Törnqvist et al., 2008; Horton and Shennan, 2009). However, there is no difference in the elevation between basal and intercalated index points in regions #2, 3, and 4, which have data covering the same time period (Fig. 3). These results contradict conclusions made from coastal organic sediments of eastern and southwestern England (Edwards, 2006; Horton and Shennan, 2009), and the Gulf coast of United States (Törnqvist et al., 2008), which show long-term compaction rates between ~0.4 and 5 mm yr^{-1}. Furthermore, Horton et al. (2013) and Khan et al. (2017) assessed the influence of compaction in organic sediments from temperate salt marshes and tropical mangroves in terms of their stratigraphic position and showed ~0.3 m compaction per meter of overburden. RSL reconstructions from intercalated samples in regions #2 and 3 from the ACE exhibit up to 8 and 9 m overburden, respectively, but do not seem to have suffered significant consolidation. Compaction parameters such as pore space, de-watering, structural collapse or biological decay of vegetal remains, and biogeochemical alteration of organic matter (van Asselen et al., 2009; Brain et al., 2017) are controlled both directly and indirectly by organic matter content (Plater et al., 2015). The coastal sediments of the ACE are minerogenic (Cearreta et al., 2013; García-Artola et al., 2016). Indeed, natural and regenerated salt-marsh sediments from the ACE contain low organic matter content (<10%), which decreases with depth due to rapid degradation at the surface (Cearreta et al., 2002, 2013; Santín et al., 2009; Fernández et al., 2010), compared to the organic-rich salt marshes of the US Atlantic coast (e.g., >40% organic matter in New England; Carey et al., 2017).

5.2. Rate of RSL rise during the Holocene from the Atlantic coast of Europe

The database from the ACE documents a continuous rise in RSL from −36.7 ± 1.2 m at ~11.5 ka until present (region #12; Fig. 4). The height of RSL did not exceed the current position at any time during the Holocene, although Moura et al. (2007) suggested a RSL highstand occurred during the mid-Holocene in southern Portugal. We analyzed the temporal variability of RSL rise for each site calculating the average rate in time intervals of 1-ka (Table 4 and Fig. 5) using the spatio-temporal empirical hierarchical model (Kopp et al., 2016). Rates of Holocene RSL rise were faster in the early Holocene (10–7 ka) with rates between 6.3 ± 0.8 mm yr^{-1} and 6.8 ± 0.5 mm yr^{-1}, and a notable decrease in rates occurred at 7 ka. This inflection in the rate of RSL rise was also observed by Vis et al. (2008), Leorri et al. (2012a,b), Stéphan and Goslin (2014), and Costas et al. (2016). The rate of RSL rise further decreased from the mid to late Holocene; from 7 to 4 ka RSL rise ranged from 1.8 ± 0.5 mm yr^{-1} to 0.5 ± 0.4 mm yr^{-1} compared to 0.9 ± 0.4 mm yr^{-1} to 0.1 ± 0.5 mm yr^{-1} between 4 ka and present. The rate of RSL rise decreased throughout the Holocene because of a reduction in meltwater input and diminishing contribution of GIA (Engelhart and Horton, 2012). The decrease in rates of RSL rise after ~7 ka coincides with the disappearance of the far-field Laurentide Ice Sheet (Carlson et al., 2008; Lambeck et al., 2014; Ullman et al., 2016), and the deglaciation peak of West Greenland (Sinclair et al., 2016). However, there is no consensus on the termination of Holocene global meltwater input, which has been associated with melting from the Antarctic Ice Sheet after ~7 ka (Nakada and Lambeck, 1988; Ivins and James, 2005; Bentley et al., 2014). Models for the end of Antarctic melting vary between 6 ka (Milne et al., 2005) and 4 ka (Peltier, 2004), or a much later melting up to 2 ka (Nakada and Lambeck, 1988; Fleming et al., 1998; Whitehouse et al., 2012; Lambeck et al., 2014) and 1 ka (Ivins et al., 2013; Bradley et al., 2016).

5.3. Spatial variability in RSL and comparison with glacial isostatic model predictions

The most likely source of spatial variability of RSL along the ACE is the deglaciation of the British-Irish and Fennoscandian Ice sheets (Carlson and Clark, 2012; Cuzzone et al., 2016). The ACE database seems to reflect the migration of the European peripheral forebulge from the northeast to the northwest during the Holocene (Fig. 5). From 8 to 4 ka, RSL rise rates decrease towards the southwest from a maximum of 2.5 ± 0.5 mm yr^{-1} (region #1) to a minimum of 1.5 ± 0.4 mm yr^{-1} (regions #8–12) (Table 4). After 4 ka, the rate of

Table 4
Rates of RSL change (±2 standard deviations) along the Atlantic coast of Europe at 1-ka time intervals estimated by the empirical hierarchical model since 11 ka.

Site	Average rate (mm yr^{-1})										
	11-10 ka	10-9 ka	9-8 ka	8-7 ka	7-6 ka	6-5 ka	5-4 ka	4-3 ka	3-2 ka	2-1 ka	1-0 ka
#1 French Flanders and Picardy coastal plain	8.4 ± 2.0	8.2 ± 1.7	6.9 ± 1.4	4.5 ± 1.0	2.6 ± 0.9	1.5 ± 0.9	1.4 ± 0.8	1.2 ± 0.8	0.6 ± 0.9	0.7 ± 1.0	0.8 ± 1.7
#2 Seine estuary and Coast of Calvados	8.5 ± 2.0	8.2 ± 1.7	6.9 ± 1.3	4.3 ± 1.0	2.3 ± 0.8	1.3 ± 0.8	1.2 ± 0.7	1.1 ± 0.7	0.5 ± 0.8	0.7 ± 0.8	0.7 ± 1.6
#3 Normano-breton Gulf and North Brittany	8.6 ± 2.0	8.3 ± 1.6	6.8 ± 1.3	4.1 ± 0.9	2.0 ± 0.8	1.0 ± 0.7	1.0 ± 0.7	1.1 ± 0.7	0.5 ± 0.7	0.6 ± 0.7	0.7 ± 1.6
#4 West Brittany	8.5 ± 1.9	8.2 ± 1.6	6.7 ± 1.3	3.9 ± 1.0	1.8 ± 0.7	0.8 ± 0.6	1.0 ± 0.5	1.2 ± 0.6	0.7 ± 0.6	0.8 ± 0.6	0.8 ± 1.5
#5 South Brittany	8.7 ± 1.9	8.3 ± 1.6	6.7 ± 1.3	3.9 ± 0.9	1.8 ± 0.7	0.8 ± 0.6	0.9 ± 0.6	1.1 ± 0.6	0.5 ± 0.6	0.6 ± 0.7	0.7 ± 1.5
#6 Coast of Vendée	8.8 ± 1.9	8.4 ± 1.6	6.7 ± 1.2	3.8 ± 0.9	1.6 ± 0.7	0.6 ± 0.7	0.6 ± 0.6	0.7 ± 0.6	0.3 ± 0.6	0.4 ± 0.7	0.6 ± 1.5
#7 Coast of Charentes	8.8 ± 1.9	8.4 ± 1.6	6.8 ± 1.3	3.8 ± 0.9	1.6 ± 0.8	0.5 ± 0.8	0.5 ± 0.7	0.6 ± 0.6	0.2 ± 0.7	0.5 ± 0.8	0.6 ± 1.6
#8 Basque Country	8.8 ± 1.9	8.4 ± 1.5	6.8 ± 1.2	3.7 ± 0.9	1.4 ± 0.8	0.3 ± 0.8	0.4 ± 0.6	0.6 ± 0.5	0.3 ± 0.5	0.6 ± 0.8	0.7 ± 1.6
#9 Asturias	8.8 ± 1.8	8.4 ± 1.4	6.8 ± 1.1	3.8 ± 0.9	1.4 ± 0.8	0.4 ± 0.8	0.5 ± 0.7	0.8 ± 0.7	0.5 ± 0.7	0.7 ± 0.7	0.8 ± 1.5
#10 Galicia	8.9 ± 1.8	8.5 ± 1.4	7.0 ± 1.1	3.9 ± 0.9	1.4 ± 0.8	0.4 ± 0.8	0.4 ± 0.7	0.7 ± 0.7	0.4 ± 0.8	0.6 ± 0.7	0.7 ± 1.5
#11 Southern Galicia and north of Portugal	9.0 ± 1.8	8.6 ± 1.4	7.1 ± 1.1	4.0 ± 0.9	1.4 ± 0.8	0.3 ± 0.8	0.3 ± 0.8	0.5 ± 0.7	0.3 ± 0.7	0.5 ± 0.6	0.6 ± 1.4
#12 Lisbon and Tagus Valley	9.2 ± 1.6	8.9 ± 1.3	7.4 ± 1.0	4.2 ± 0.7	1.5 ± 0.8	0.2 ± 0.8	0.0 ± 0.7	0.1 ± 0.7	−0.2 ± 0.7	0.1 ± 0.8	0.3 ± 1.6
#13 Algarve	9.0 ± 1.7	8.8 ± 1.4	7.4 ± 1.1	4.5 ± 0.7	2.0 ± 0.7	0.7 ± 0.7	0.5 ± 0.6	0.5 ± 0.6	0.1 ± 0.6	0.3 ± 0.7	0.4 ± 1.6

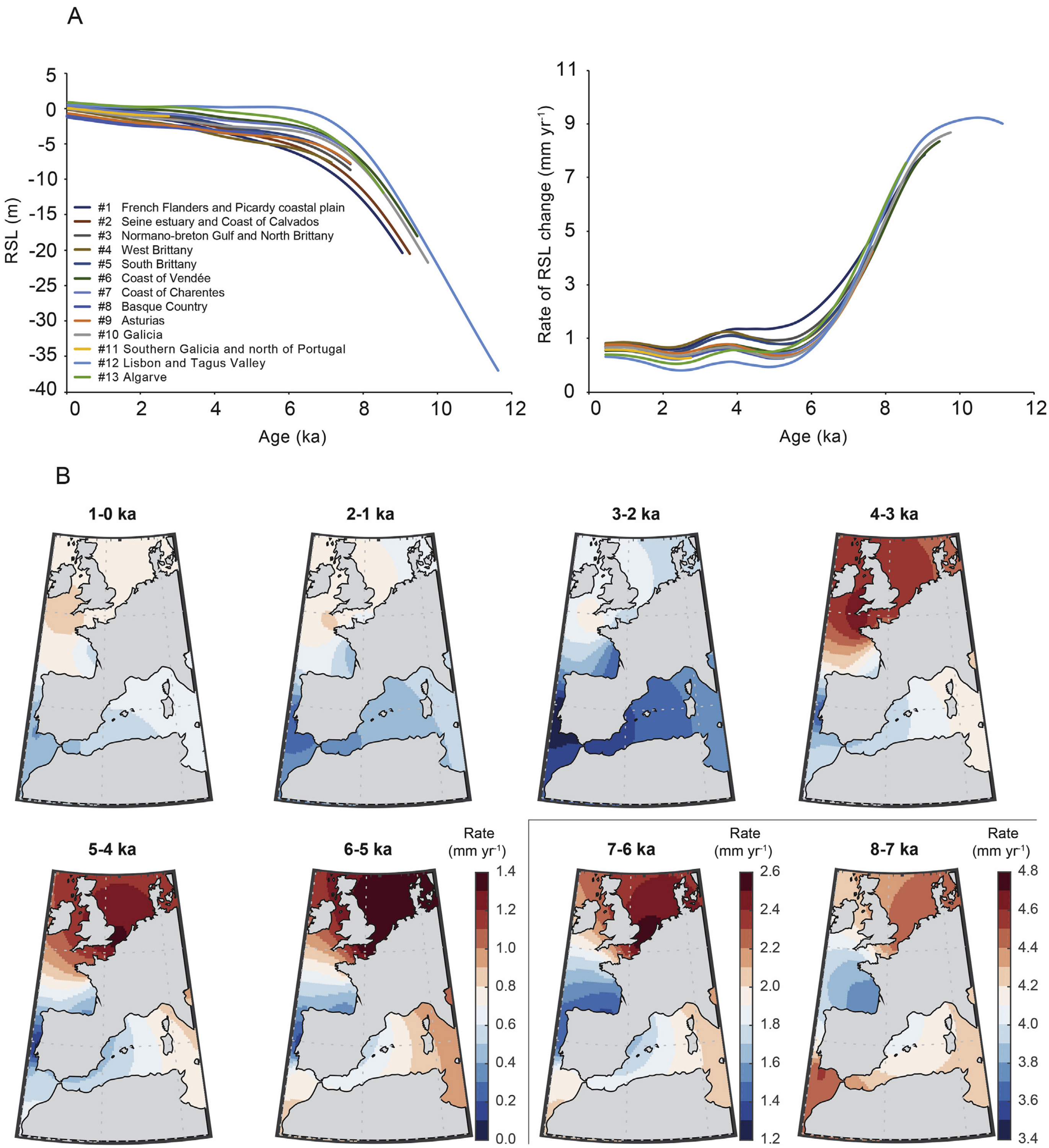

Fig. 5. Mean estimates of RSL heights and rates of change from the spatio-temporal model for each coastal region (A) and rates of RSL change for the entire Atlantic coast of Europe in 1-ka time intervals (B). Note the changes of scale among time intervals.

RSL rise decreases from the northwest (0.9 ± 0.4 mm yr^{-1}; region #4) to a minimum of 0.1 ± 0.5 mm yr^{-1} (region #12). These results confirm previous conclusions showing highest RSL rates associated with the peak forebulge collapse occurring in distal locations, up to hundreds of kilometers away from the former ice margins (Farrell and Clark, 1976; Engelhart and Horton, 2012; Engelhart et al., 2015). Data from regions #12 and 13 do not follow the general north-south trend and present higher rates to the south in region #13 (Fig. 5). Previous regional studies in Algarve/Gulf of Cadiz area have also suggested anomalously high rates of Holocene RSL rise (Dabrio et al., 2000; Delgado et al., 2012). Consequently, RSL records from the southern region of Portugal could be influenced by the previously mentioned late Quaternary tectonic activity as suggested by Leorri et al. (2012a,b).

GIA model predictions have been compared to RSL reconstructions from the ACE (Leorri et al., 2012a,b; Goslin et al., 2015; Costas et al., 2016). Similar to Bradley et al. (2011), the predictions of the GIA model used here (Bradley et al., 2016 with the rheological parameters from Leorri et al., 2012a,b) compare favorably at most regions during the Holocene. However, misfits are observed before ~7 ka in regions #6, 10, 12, and 13; the RSL reconstruction is up to ~10 m below GIA model predictions at ~9 ka in region #6 (Fig. 3). Furthermore, region #8 also shows late Holocene RSL reconstructions ~2.5 m below the GIA model predictions (Fig. 4). However, many salt marshes from the Basque Country studied in this database have suffered land drainage related to reclamation for agricultural purposes (e.g., Pascual et al., 2000), which would have led to compaction and lower the RSL reconstructions in this area (Shennan and Horton, 2002).

Other possible causes of discrepancies between the RSL records and GIA model predictions have been extensively discussed in previous studies (Leorri et al., 2012a,b; Goslin et al., 2015). These differences could be caused by changes in paleo-tidal ranges at regional (continental shelf) and local (bay, estuary) scales (region #4), tectonic activity (region #13), and large morphological coastal changes (region #7). Otherwise, uncertainties in GIA models employed have been pointed out, such as the choice of parameters for the Earth model used (especially the lithosphere thickness and mantle viscosity structure) and the deglaciation history of the Fennoscandian ice sheet (Goslin et al., 2015).

6. Conclusions

We produced a standardized Holocene RSL database from the Atlantic coast of Europe (ACE) that synthesizes the existing results from northern France to southern Portugal. The database is based upon 214 index points and 126 limiting dates that extend back to ~11.5 ka. The ACE represents an intermediate-field location with a continuous Holocene RSL rise history controlled by isostatic and eustatic factors. We observed the highest rates of RSL change in the early Holocene (10–7 ka) with a maximum in middle Portugal (6.8 ± 0.5 mm yr^{-1}) and a minimum in southwestern France (6.3 ± 0.8 mm yr^{-1}). Reduction of meltwater input explains the slowdown in the rates after 7 ka, up to 0.1 ± 0.5 mm yr^{-1} in middle Portugal during the late Holocene. The spatial variability of the ACE database reflects the deglaciation of the British-Irish and Fennoscandian Ice Sheets and the migration of the peripheral forebulge from a northeast position before ~4 ka to a northwest location in the late Holocene.

Acknowledgments

AGA received a postdoctoral grant from the Basque Government (POS-2014-1-51). AC and AGA were supported by Antropicosta (MINECO, CGL2013-41083-P), Harea-Coastal Geology Research Group (EJ/GV, IT976-16) and Quaternary Unit for Research and Education (UPV/EHU, UFI11/09) grants. REK was supported in part by NSF grants OCE-1458904 and OCE-1702587. BPH was supported by Singapore Ministry of Education Academic Research Fund Tier 1 RG119/17, the National Research Foundation Singapore, and the Singapore Ministry of Education, under the Research Centres of Excellence initiative. We are grateful to Professor Glenn A. Milne for providing GIA predictions and helpful comments on the manuscript. We thank Ángela Alonso and José Luis Pagés, former professors at the Universidade de A Coruña, for providing their data from Asturias and Galicia and assisting us in the reinterpretation of their previous results to follow the standards of the database. The authors also thank two anonymous reviewers for their thoughtful comments and helpful reviews. This paper is a contribution to INQUA Project 1601P, IGCP Projects 588 and 639, PALSEA, Earth Observatory of Singapore (#203) and Geo-Q Zentroa Research Unit (paper #48 of the Joaquín Gómez de Llarena Laboratory).

Appendix A. Supplementary data

Supplementary data related to this article can be found at https://doi.org/10.1016/j.quascirev.2018.07.031.

References

Admiralty Tide Tables, 2015. Europe (Excluding United Kingdom and Ireland), Mediterranean Sea and Atlantic Ocean, 2. United Kingdom Hydrographic Office, Taunton.
Alonso, A., Pagés, J.L., 2000. El registro sedimentario del final del Cuaternario en el litoral noroeste de la Península Ibérica. Márgenes cantábrico y atlántico. Rev. Soc. Geol. Esp 13, 17–29.
Alonso, A., Pagés, J.L., 2010. Evolución del nivel del mar durante el Holoceno en el noroeste de la Península Ibérica. Rev. Soc. Geol. Esp 23, 157–167.
Ashe, E.L., Cahill, N., Hay, C.C., Khan, N.S., Kemp, A.C., Engelhart, S.E., Horton, B.P., Parnell, A.C., Kopp, R.E., in review. Statistical modeling of rates and trends in sea level. Quat. Sci. Rev..
Bao, R., Freitas, M.C., Andrade, C., 1999. Separating eustatic from local environmental effects: a late-Holocene record of coastal change in Albufeira Lagoon, Portugal. Holocene 9, 341–352.
Baptista, M.A., Miranda, J.M., Chierici, F., Zitellini, N., 2003. New study of the 1755 earthquake source based on multi-channel seismic survey data and tsunami modeling. Nat. Hazards Earth Syst. Sci. 3, 333–340.
Benito, I., Onaindia, M., 1991. Estudio de la distribución de las plantas halófilas y su relación con los factores ambientales en la marisma de Mundaka-Urdaibai. Implicaciones en la gestión del medio natural. Cuadernos de Sección (Ciencias Naturales) de Eusko Ikaskuntza 8, 1–116.
Bentley, M.J., Ó Cofaigh, C., Anderson, J.B., Conway, H., Davies, B., Graham, A.G.C., Hillenbrand, C.-D., Hodgson, D.A., Jamieson, S.S.R., Larter, R.D., Mackintosh, A., Smith, J.A., Verleyen, E., Ackert, R.P., Bart, P.J., Berg, S., Brunstein, D., Canals, M., Colhoun, E.A., Crosta, X., Dickens, W.A., Domack, E., Dowdeswell, J.A., Dunbar, R., Ehrmann, W., Evans, J., Favier, V., Fink, D., Fogwill, C.J., Glasser, N.F., Gohl, K., Golledge, N.R., Goodwin, I., Gore, D.B., Greenwood, S.L., Hall, B.L., Hall, K., Hedding, D.W., Hein, A.S., Hocking, E.P., Jakobsson, M., Johnson, J.S., Jomelli, V., Jones, R.S., Klages, J.P., Kristoffersen, Y., Kuhn, G., Leventer, A., Licht, K., Lilly, K., Lindow, J., Livingstone, S.J., Massé, G., McGlone, M.S., McKay, R.M., Melles, M., Miura, H., Mulvaney, R., Nel, W., Nitsche, F.O., O'Brien, P.E., Post, A.L., Roberts, S.J., Saunders, K.M., Selkirk, P.M., Simms, A.R., Spiegel, C., Stolldorf, T.D., Sugden, D.E., van der Putten, N., van Ommen, T., Verfaillie, D., Vyverman, W., Wagner, B., White, D.A., Witus, A.E., Zwartz, D., 2014. A community-based geological reconstruction of Antarctic ice sheet deglaciation since the last glacial maximum. Quat. Sci. Rev. 100, 1–9.
Besana-Ostman, G.M., Vilanova, S.P., Nemser, E.S., Falcao-Flor, A., Heleno, S., Ferreira, H., Fonseca, J.D., 2012. Large Holocene earthquakes in the lower Tagus Valley fault zone, Central Portugal. Seismol Res. Lett. 83, 67–76.
Billeaud, I., 2007. Dynamique de construction d'un prisme sédimentaire littoral en régime mégatidal (la Baie du Mont-Saint-Michel). Ph.D. thesis. Université de Caen Normandie.
Boillot, G., Dupeuble, P.A., Malod, J., 1979. Subduction and tectonics on the continental margin off northern Spain. Mar. Geol. 32, 53–70.
Boski, T., Moura, D., Veiga-Pires, C., Camacho, S., Duarte, D., Scott, D.B., Fernandes, S.G., 2002. Postglacial sea-level rise and sedimentary response in the Guadiana Estuary, Portugal/Spain border. Sediment. Geol. 150, 103–122.
Bradley, S.L., Milne, G.A., Horton, B.P., Zong, Y., 2016. Modelling sea level data from China and Malay-Thailand to estimate Holocene ice-volume equivalent sea level change. Quat. Sci. Rev. 137, 54–68.
Bradley, S.L., Milne, G.A., Shennan, I., Edwards, R., 2011. An improved glacial isostatic adjustment model for the British Isles. J. Quat. Sci. 26, 541–552.
Brain, M.J., Kemp, A.C., Hawkes, A.D., Engelhart, S.E., Vane, C.H., Cahill, N., Hill, T.D., Donnelly, J.P., Horton, B.P., 2017. Exploring mechanisms of compaction in salt-marsh sediments using Common Era relative sea-level reconstructions. Quat. Sci. Rev. 167, 96–111.
Brain, M.J., Long, A.J., Petley, D.N., Horton, B.P., Allison, R.J., 2011. Compression behaviour of minerogenic low energy intertidal sediments. Sediment. Geol. 233, 28–41.
Brooks, A., Edwards, R., 2006. The development of A sea-Level database for Ireland. Ir. J. Earth Sci. 24, 13–27.
Camacho, S., Boski, T., Moura, D., Scott, D., Connor, S., Pereira, L., 2017. Paleoenvironmental evolution of the Guadiana Estuary, Portugal, during the Holocene: a modern foraminifera analog approach. Holocene 27, 197–235.
Carey, J.C., Moran, S.B., Kelly, R.P., Kolker, A.S., Fulweiler, R.W., 2017. The declining role of organic matter in new England salt marshes. Estuar. Coast 40, 626–639.
Carlson, A.E., Clark, P.U., 2012. Ice sheet sources of sea level rise and freshwater discharge during the last deglaciation. Rev. Geophys. 50, RG4007.
Carlson, A.E., LeGrande, A.N., Oppo, D.W., Came, R.E., Schmidt, G.A., Anslow, F.S., Licciardi, J.M., Obbink, E.A., 2008. Rapid early Holocene deglaciation of the

Laurentide ice sheet. Nat. Geosci. 1, 620–624.
Cearreta, A., 1998. Holocene sea-level change in the Bilbao estuary (north Spain): foraminiferal evidence. Micropaleontology 44, 265–276.
Cearreta, A., Cachão, M., Cabral, M.C., Bao, R., Ramalho, M.J., 2003. Lateglacial and Holocene environmental changes in Portuguese coastal lagoons 2: microfossil multiproxy reconstruction of the Santo André coastal area. Holocene 13, 447–458.
Cearreta, A., García-Artola, A., Leorri, E., Irabien, M.J., Masque, P., 2013. Recent environmental evolution of regenerated salt marshes in the southern Bay of Biscay: anthropogenic evidences in their sedimentary record. J. Mar. Syst. 109–110, S203–S212.
Cearreta, A., Irabien, M.J., Ulibarri, I., Yusta, I., Croudace, I.W., Cundy, A.B., 2002. Recent salt marsh development and natural regeneration of reclaimed areas in the plentzia estuary. N. Spain. Estuar. Coast Shelf Sci. 54, 863–886.
Cearreta, A., Monge-Ganuzas, M., 2013. Evolución paleoambiental del estuario del Oka (Reserva de la Biosfera de Urdaibai, Vizcaya): respuesta al ascenso del nivel marino durante el Holoceno. Geotemas 14, 163–166.
Cearreta, A., Murray, J.W., 2000. AMS 14C dating of Holocene estuarine deposits: consequences of high energy and reworked foraminifera. Holocene 10, 155–159.
Chaumillon, E., Tessier, B., Reynaud, J.Y., 2010. Stratigraphic records and variability of incised valleys and estuaries along French coasts. Bull. Soc. Geol. Fr. 181, 75–85.
Chen, X., Zhang, X., Church, J.A., Watson, C.S., King, M.A., Monselesan, D., Legresy, B., Harig, C., 2017. The increasing rate of global mean sea-level rise during 1993-2014. Nat. Clim. Change 7, 492–495.
Chester, D.K., 2001. The 1755 Lisbon earthquake. Prog. Phys. Geogr. 25, 363–383.
Church, J.A., Clark, P.U., Cazenave, A., Gregory, J.M., Jevrejeva, S., Levermann, A., Merrifield, M.A., Milne, G.A., Nerem, R.S., Nunn, P.D., Payne, A.J., Pfeffer, W.T., Stammer, D., Unnikrishnan, A.S., 2013. sea-level rise by 2100. Science 342, 1445–1445.
Clark, C.D., Hughes, A.L.C., Greenwood, S.L., Jordan, C., Sejrup, H.P., 2012. Pattern and timing of retreat of the last British-Irish ice sheet. Quat. Sci. Rev. 44, 112–146.
Clavé, B., Massé, L., Carbonel, P., Tastet, J.-P., 2001. Holocene coastal changes and infilling of the La Perroche marsh (French Atlantic coast). Oceanol. Acta 24, 377–389.
Costas, S., Ferreira, Ó., Plomaritis, T.A., Leorri, E., 2016. Coastal barrier stratigraphy for Holocene high-resolution sea-level reconstruction. Sci. Rep. 6, 38726.
Cressie, N., Wikle, C.K., 2011. Statistics for Spatio-temporal Data. John Wiley & Sons, Ltd, Hoboken, NJ.
Cuzzone, J.K., Clark, P.U., Carlson, A.E., Ullman, D.J., Rinterknecht, V.R., Milne, G.A., Lunkka, J.-P., Wohlfarth, B., Marcott, S.A., Caffee, M., 2016. Final deglaciation of the Scandinavian Ice Sheet and implications for the Holocene global sea-level budget. Earth Planet Sci. Lett. 448, 34–41.
Dabrio, C.J., Zazo, C., Goy, J.L., Sierro, F.J., Borja, F., Lario, J., González, J.A., Flores, J.A., 2000. Depositional history of estuarine infill during the last postglacial transgression (Gulf of Cadiz, Southern Spain). Mar. Geol. 162, 381–404.
de Groot, T.A.M., Granja, H.M., 1998. Coastal environments, sea-level and neotectonism from cored boreholes (northwest Portugal): preliminary results. J. Coastal Res. Special Issue 26, 115–124.
Delgado, J., Boski, T., Nieto, J.M., Pereira, L., Moura, D., Gomes, A., Sousa, C., Garcia-Tenorio, R., 2012. Sea-level rise and anthropogenic activities recorded in the late Pleistocene/Holocene sedimentary infill of the Guadiana Estuary (SW Iberia). Quat. Sci. Rev. 33, 121–141.
Dias, J.M.A., Boski, T., Rodrigues, A., Magalhaes, F., 2000. Coast line evolution in Portugal since the Last Glacial Maximum until present - a synthesis. Mar. Geol. 170, 177–186.
Dias, R.P., 2001. Neotectónica da Região do Algarve. Ph.D. thesis. Universidade de Lisboa.
Edwards, R.J., 2006. Mid- to late-Holocene relative sea-level change in southwest Britain and the influence of sediment compaction. Holocene 16, 575–587.
Engelhart, S.E., Horton, B.P., 2012. Holocene sea level database for the Atlantic coast of the United States. Quat. Sci. Rev. 54, 12–25.
Engelhart, S.E., Peltier, W.R., Horton, B.P., 2011. Holocene relative sea-level changes and glacial isostatic adjustment of the U.S. Atlantic coast. Geology 39, 751–754.
Engelhart, S.E., Vacchi, M., Horton, B.P., Nelson, A.R., Kopp, R.E., 2015. A sea-level database for the Pacific coast of central North America. Quat. Sci. Rev. 113, 78–92.
Farrell, W.E., Clark, J.A., 1976. On postglacial sea level. Geophys. J. Roy. Astron. Soc. 46, 647–667.
Fatela, F., Moreno, J., Moreno, F., Araújo, M.F., Valente, T., Antunes, C., Taborda, R., Andrade, C., Drago, T., 2009. Environmental constraints of foraminiferal assemblages distribution across a brackish tidal marsh (Caminha, NW Portugal). Mar. Micropaleontol. 70, 70–88.
Fenies, H., Lericolais, G., Posamentier, H.W., 2010. Comparison of wave-and tide-dominated incised valleys: specific processes controlling systems tract architecture and reservoir geometry. Bull. Soc. Geol. Fr. 181, 171–181.
Fernández, S., Santín, C., Marquínez, J., Álvarez, M.A., 2010. Saltmarsh soil evolution after land reclamation in Atlantic estuaries (Bay of Biscay, North coast of Spain). Geomorphology 114, 497–507.
Fleming, K., Johnston, P., Zwartz, D., Yokoyama, Y., Lambeck, K., Chappell, J., 1998. Refining the eustatic sea-level curve since the Last Glacial Maximum using far-and intermediate-field sites. Earth Planet Sci. Lett. 163, 327–342.
Freitas, M.C., Andrade, C., Rocha, F., Tassinari, C., Munhá, J.M., Cruces, A., Vidinha, J., Silva, C.M.d, 2003. Lateglacial and Holocene environmental changes in Portuguese coastal lagoons 1: the sedimentological and geochemical records of the Santo André coastal area. Holocene 13, 433–446.
Frouin, M., Durand, A., Sebag, D., Huault, M.-F., Ogier, S., Verrecchia, E.P., Laignel, B., 2009. Holocene evolution of a wetland in the lower seine valley, marais Vernier, France. Holocene 19, 717–727.
Gabet, C., 1973. Le banc de tourbe sur l'estran de la baie de Perroche (Île d'Oléron). Recueil de la Société d'archéologie et d'histoire de la Charente - Maritime 25, 297–307.
Gandouin, E., Ponel, P., Andrieu-Ponel, V., Guiter, F., de Beaulieu, J.-L., Djamali, M., Franquet, E., Van Vliet-Lanoë, B., Alvitre, M., Meurisse, M., Brocandel, M., Brulhet, J., 2009. 10,000 years of vegetation history of the Aa palaeoestuary, St-Omer Basin. northern France. Rev. Palaeobot. Palynol 156, 307–318.
Gandouin, E., Van Vliet Lanoe, B., Franquet, E., Andrieu-Ponel, V., Keen, D.H., Ponel, P., Meurisse, M., Brulhet, J., Brocandel, M., 2007. Analyse en haute résolution de l'enregistrement de la transgression holocène dans un secteur subsident du littoral français: le bassin-marais de Saint-Omer (Pas-de-Calais, France). Géologie de la France 1, 11–32.
García-Artola, A., Cearreta, A., Irabien, M.J., Leorri, E., Sanchez-Cabeza, J.-A., Corbett, D.R., 2016. Agricultural fingerprints in salt-marsh sediments and adaptation to sea-level rise in the eastern Cantabrian coast (N. Spain). Estuar. Coast Shelf Sci. 171, 66–76.
García-Artola, A., Cearreta, A., Leorri, E., 2015. Relative sea-level changes in the Basque coast (northern Spain, Bay of Biscay) during the Holocene and Anthropocene: the Urdaibai estuary case. Quat. Int. 364, 172–180.
Goslin, J., Van Vliet Lanoë, B., Spada, G., Bradley, S., Tarasov, L., Neill, S., Suanez, S., 2015. A new Holocene relative sea-level curve for western Brittany (France): insights on isostatic dynamics along the Atlantic coasts of north-western Europe. Quat. Sci. Rev. 129, 341–365.
Goslin, J., Van Vliet-Lanoë, B., Stéphan, P., Delacourt, C., Fernane, A., Gandouin, E., Hénaff, A., Penaud, A., Suanez, S., 2013. Holocene relative sea-level changes in western Brittany (France) between 7600 and 4000 cal. BP: reconstitution from basal-peat deposits. Géomorphologie 19, 425–444.
Hernández Martín, S., 2013. Evolución ambiental de los estuarios vascos (Urdaibai y Deba) durante el Holoceno como consecuencia del ascenso del nivel marino. CKQ Estudios de Cuaternario 3, 51–63.
Hijma, M.P., Engelhart, S.E., Törnqvist, T.E., Horton, B.P., Hu, P., Hill, D.F., 2015. A protocol for a geological sea-level database. In: Shennan, I., Long, A.J., Horton, B.P. (Eds.), Handbook of Sea-level Research. John Wiley & Sons, Ltd, Chichester, pp. 536–553.
Hill, D.F., 2016. Spatial and temporal variability in tidal range: evidence, causes, and effects. Curr. Clim. Change Rep 2, 232–241.
Hinkel, J., Jaeger, C., Nicholls, R.J., Lowe, J., Renn, O., Peijun, S., 2015. Sea-level rise scenarios and coastal risk management. Nat. Clim. Change 5, 188–190.
Horton, B.P., Corbett, R., Culver, S.J., Edwards, R.J., Hillier, C., 2006. Modern saltmarsh diatom distributions of the Outer Banks, North Carolina, and the development of a transfer function for high resolution reconstructions of sea level. Estuar. Coast Shelf Sci. 69, 381–394.
Horton, B.P., Edwards, R.J., Lloyd, J.M., 2000. Implications of a microfossil-based transfer function in Holocene sea-level studies. Geol. Soc. London Special Publication 166, 41–54.
Horton, B.P., Engelhart, S.E., Hill, D.F., Kemp, A.C., Nikitina, D., Miller, K.G., Peltier, W.R., 2013. Influence of tidal-range change and sediment compaction on Holocene relative sea-level change in New Jersey, USA. J. Quat. Sci. 28, 403–411.
Horton, B.P., Gibbard, P., Mine, G., Morley, R., Purintavaragul, C., Stargardt, J., 2005. Holocene sea levels and palaeoenvironments, Malay-Thai Peninsula, southeast Asia. Holocene 15, 1199–1213.
Horton, B.P., Kopp, R.E., Garner, A.J., Hay, C.C., Khan, N.S., Roy, K., Shaw, T.A., 2018. Mapping sea-level change in time, space, and probability. Annu. Rev. Environ. Resour. in press.
Horton, B.P., Shennan, I., 2009. Compaction of Holocene strata and the implications for relative sea-level change on the east coast of England. Geology 37, 1083–1086.
Hu, P., 2010. Developing a Quality-controlled Postglacial Sea-level Database for Coastal Louisiana to Assess Conflicting Hypotheses of Gulf Coast Sea-level Change. M.Sc. thesis. Tulane University.
Huault, M.F., 1980. Nouvelles recherches palynologiques sur le Marais Vernier. Bull. Assoc. Fr. Etud. Quat 17, 53–56.
Huault, M.F., 1985. Apports des diatomées à la reconstitution des paléoenvironnentents: l'exemple du Marais Vernier lors de la transgression flandrienne. Bull. Assoc. Fr. Etud. Quat 22, 209–217.
Ivins, E.R., James, T.S., 2005. Antarctic glacial isostatic adjustment: a new assessment. Antarct. Sci. 17, 541–553.
Ivins, E.R., James, T.S., Wahr, J., Schrama, E.J.O., Landerer, F.W., Simon, K.M., 2013. Antarctic contribution to sea level rise observed by GRACE with improved GIA correction. J. Geophys. Res. B: Solid Earth 118, 3126–3141.
Jelgersma, S., 1961. Holocene Sea Level Changes in the Netherlands. Van Aelst, Maastricht.
Joly, C., 2004. Histoire végétale d'une tourbière littorale: le marais des Bourbes (Olonnesur-Mer, Vendée). Ann. Paleontol. 90, 187–207.
Joly, C., Visset, L., 2009. Evolution of vegetation landscapes since the late mesolithic on the French west Atlantic coast. Rev. Palaeobot. Palynol. 154, 124–179.
Kemp, A.C., Horton, B.P., Corbett, D.R., Culver, S.J., Edwards, R.J., van de Plassche, O., 2009. The relative utility of foraminifera and diatoms for reconstructing late Holocene sea-level change in North Carolina, USA. Quat. Res. (Duluth) 71, 9–21.
Kemp, A.C., Vane, C.H., Horton, B.P., Culver, S.J., 2010. Stable carbon isotopes as

potential sea-level indicators in salt marshes, North Carolina, USA. Holocene 20, 623–636.
Khan, N.S., Ashe, E., Horton, B.P., Dutton, A., Kopp, R.E., Brocard, G., Engelhart, S.E., Hill, D.F., Peltier, W.R., Vane, C.H., Scatena, F.N., 2017. Drivers of Holocene Sea-level change in the Caribbean. Quat. Sci. Rev. 155, 13–36.
Khan, N.S., Ashe, E., Shaw, T.A., Vacchi, M., Walker, J., Peltier, W.R., Kopp, R.E., Horton, B.P., 2015. Holocene relative sea-Level changes from near-, intermediate-, and far-field locations. Curr. Clim. Change Rep 1, 247–262.
Klingebiel, A., Gayet, J., 1995. Fluvio-lagoonal sedimentary sequences in Leyre delta and Arcachon bay, and Holocene sea level variations, along the Aquitaine coast (France). Quat. Int. 29, 111–117.
Kopp, R.E., 2016. CESL-stehm-gp (Version 1.0). Computer software. http://github.com/bobkopp/CESL-STEHM-GP. (Accessed 3 March 2018).
Kopp, R.E., Hay, C.C., Little, C.M., Mitrovica, J.X., 2015. Geographic variability of sea-Level change. Curr. Clim. Change Rep 1, 192–204.
Kopp, R.E., Kemp, A.C., Bittermann, K., Horton, B.P., Donnelly, J.P., Gehrels, W.R., Hay, C.C., Mitrovica, J.X., Morrow, E.D., Rahmstorf, S., 2016. Temperature-driven global sea-level variability in the Common Era. Proc. Natl. Acad. Sci. U.S.A. 113, E1434–E1441.
Lambeck, K., Rouby, H., Purcell, A., Sun, Y., Sambridge, M., 2014. sea level and global ice volumes from the last glacial maximum to the Holocene. Proc. Natl. Acad. Sci. U.S.A. 111, 15296–15303.
Lambeck, K., Smither, C., Johnston, P., 1998. Sea-level change, glacial rebound and mantle viscosity fornorthern Europe. Geophys. J. Int. 134, 102–144.
Leorri, E., Cearreta, A., Milne, G., 2012a. Field observations and modelling of Holocene sea-level changes in the southern Bay of Biscay: implication for understanding current rates of relative sea-level change and vertical land motion along the Atlantic coast of SW Europe. Quat. Sci. Rev. 42, 59–73.
Leorri, E., Fatela, F., Drago, T., Bradley, S.L., Moreno, J., Cearreta, A., 2012b. Lateglacial and Holocene coastal evolution in the Minho estuary (N Portugal): implications for understanding sea-level changes in Atlantic Iberia. Holocene 23, 353–363.
Lespez, L., Clet-Pellerin, M., Davidson, R., Hermier, G., Carpentier, V., Cador, J.-M., 2010. Middle to Late Holocene landscape changes and geoarchaeological implications in the marshes of the Dives estuary (NW France). Quat. Int. 216, 23–40.
Love, R., Milne, G.A., Tarasov, L., Engelhart, S.E., Hijma, M.P., Latychev, K., Horton, B.P., Törnqvist, T.E., 2016. The contribution of glacial isostatic adjustment to projections of sea-level change along the Atlantic and Gulf coasts of North America. Earth's Future 4, 440–464.
Martins, J.M.M., Monge Soares, A.M., 2013. Marine radiocarbon reservoir effect in southern Atlantic iberian coast. Radiocarbon 55, 1123–1134.
McHutchon, A., Rasmussen, C.E., 2011. Gaussian process training with input noise. Adv. Neural Inf. Process. Syst. 24, 1341–1349.
Mengel, M., Levermann, A., Frieler, K., Robinson, A., Marzeion, B., Winkelmann, R., 2016. Future sea level rise constrained by observations and long-term commitment. Proc. Natl. Acad. Sci. U. S. A 113, 2597–2602.
Menier, D., Tessier, B., Proust, J.-N., Baltzer, A., Sorrel, P., Traini, C., 2010. The Holocene transgression as recorded by incised-valley infilling in a rocky coast context with low sediment supply (southern Brittany, western France). Bull. Soc. Geol. Fr. 181, 115–128.
Milne, G.A., Gehrels, W.R., Hughes, C.W., Tamisiea, M.E., 2009. Identifying the causes of sea-level change. Nat. Geosci. 2, 471–478.
Milne, G.A., Long, A.J., Bassett, S.E., 2005. Modelling Holocene relative sea-level observations from the Caribbean and south America. Quat. Sci. Rev. 24, 1183–1202.
Milne, G.A., Peros, M., 2013. Data–model comparison of Holocene sea-level change in the circum-Caribbean region. Global Planet. Change 107, 119–131.
Mitrovica, J.X., Milne, G.A., 2002. On the origin of late Holocene sea-level highstands within equatorial ocean basins. Quat. Sci. Rev. 21, 2179–2190.
Monge Soares, A.M., Dias, J.M.A., 2006. Coastal upwelling and radiocarbon—evidence for temporal fluctuations in ocean reservoir effect off Portugal during the Holocene. Radiocarbon 48, 45–60.
Monge Soares, A.M., Dias, J.M.A., 2007. Reservoir effect of coastal waters off western and northwestern Galicia. Radiocarbon 49, 925–936.
Monge Soares, A.M., Gutiérrez-Zugasti, I., González-Morales, M., Matos Martins, J.M., Cuenca-Solana, D., Bailey, G.N., 2016. Marine radiocarbon reservoir effect in late pleistocene and early Holocene coastal waters off northern iberia. Radiocarbon 58, 869–883.
Morzadec-Kerfourn, M.-T., 1995. Coastline changes in the Armorican massif (France) during the Holocene. J. Coastal Res. Special Issue 17, 197–203.
Moura, D., Veiga-Pires, C., Albardeiro, L., Boski, T., Rodrigues, A.L., Tareco, H., 2007. Holocene sea level fluctuations and coastal evolution in the central Algarve (southern Portugal). Mar. Geol. 237, 127–142.
Mrani-Alaoui, M., Anthony, E.J., 2011. New data and a morphodynamic perspective on mid- to late-Holocene palaeoenvironmental changes in the French Flanders coastal plain, southern North Sea. Holocene 21, 445–453.
Muhr, B., 2016. Klimadiagramme. http://www.klimadiagramme.de/. (Accessed 14 October 2017).
Nakada, M., Lambeck, K., 1988. The melting history of the late Pleistocene Antarctic ice sheet. Nature 333, 36–40.
Naughton, F., Sánchez Goñi, M.F., Drago, T., Freitas, M.C., Oliveira, A., 2007. Holocene changes in the douro estuary (northwestern iberia). J. Coast Res. 23, 711–720.
Nicholls, R.J., Hanson, S.E., Lowe, J.A., Warrick, R.A., Lu, X., Long, A.J., 2014. Sea-level scenarios for evaluating coastal impacts. Wiley Interdiscip. Rev. Clim. Change 5, 129–150.
Pascual, A., Weber, O., Rodríguez-Lázaro, J., Jouanneau, J., 2000. Evolución sedimentaria del pólder Anbeko (Reserva de Urdaibai, Golfo de Vizcaya) durante el Holoceno. Geogaceta 28, 113–116.
Peltier, W.R., 1996. Global sea level rise and glacial isostatic adjustment: an analysis of data from the east coast of North America. Geophys. Res. Lett. 23, 717–720.
Peltier, W.R., 2004. Global glacial isostasy and the surface of the ice-age earth: the ice-5G (VM2) model and grace. Annu. Rev. Earth Planet Sci. 32, 111–149.
Plater, A.J., Kirby, J.R., Boyle, J.F., Shaw, T., Mills, H., 2015. Loss on ignition and organic content. In: Shennan, I., Long, A.J., Horton, B.P. (Eds.), Handbook of Sea-level Research. John Wiley & Sons, Ltd, Chichester, pp. 312–330.
Preuss, H., 1979. Progress in computer evaluation of sea level data within the IGCP Project no. 61. In: Proceedings of the 1978 International Symposium of Coastal Evolution in the Quaternary. Sao Paulo, Brazil, pp. 104–134.
Puertos del Estado, 2014. REDMAR: red de Mareógrafos de Puertos del Estado (Informe Anual 2013). Ministerio de Fomento. http://calipso.puertos.es/BD/informes/anuales/redmar/REDMAR2013.pdf. (Accessed 9 September 2017).
Rasmussen, C.E., Williams, C.K.I., 2006. Gaussian Processes for Machine Learning. MIT Press, Cambridge, MA.
Reimer, P.J., Bard, E., Bayliss, A., Beck, J.W., Blackwell, P.G., Bronk Ramsey, C., Buck, C.E., Cheng, H., Edwards, R.L., Friedrich, M., Grootes, P.M., Guilderson, T.P., Haflidason, H., Hajdas, I., Hatté, C., Heaton, T.J., Hoffmann, D.L., Hogg, A.G., Hughen, K.A., Kaiser, K.F., Kromer, B., Manning, S.W., Niu, M., Reimer, R.W., Richards, D.A., Scott, E.M., Southon, J.R., Staff, R.A., Turney, C.S.M., van der Plicht, J., 2013. IntCal13 and Marine13 radiocarbon age calibration curves 0–50,000 Years cal BP. Radiocarbon 55, 1869–1887.
Roy, K., Peltier, W.R., 2015. Glacial isostatic adjustment, relative sea level history and mantle viscosity: reconciling relative sea level model predictions for the U.S. East coast with geological constraints. Geophys. J. Int. 201, 1154–1179.
Santín, C., de la Rosa, J.M., Knicker, H., Otero, X.L., Álvarez, M.Á., González-Vila, F.J., 2009. Effects of reclamation and regeneration processes on organic matter from estuarine soils and sediments. Org. Geochem. 40, 931–941.
Schneider, H., Höfer, D., Trog, C., Busch, S., Schneider, M., Baade, J., Daut, G., Mäusbacher, R., 2010. Holocene estuary development in the Algarve Region (Southern Portugal) – a reconstruction of sedimentological and ecological evolution. Quat. Int. 221, 141–158.
Shennan, I., 1986. Flandrian sea-level changes in the Fenland. II: tendencies of sea-level movement, altitudinal changes, and local and regional factors. J. Quat. Sci. 1, 155–179.
Shennan, I., Horton, B., 2002. Holocene land-and sea-level changes in Great Britain. J. Quat. Sci. 17, 511–526.
Shennan, I., Lambeck, K., Horton, B., Innes, J., Lloyd, J., McArthur, J., Rutherford, M., 2000. Holocene isostasy and relative sea-level changes on the east coast of England. Geol. Soc. London Special Publication 166, 275–298.
Shennan, I., Long, A.J., Horton, B.P. (Eds.), 2015. Handbook of Sea-level Research. John Wiley & Sons, Ltd, Chichester.
SHOM, 2016. Marine Altimetric References, Cotes du zéro hydrographique et niveaux caractéristiques de la marée. Edition SHOM, Brest.
Sinclair, G., Carlson, A.E., Mix, A.C., Lecavalier, B.S., Milne, G., Mathias, A., Buizert, C., DeConto, R., 2016. Diachronous retreat of the Greenland ice sheet during the last deglaciation. Quat. Sci. Rev. 145, 243–258.
Stéphan, P., Goslin, J., 2014. Evolution du niveau marin relatif à l'Holocène le long des côtes françaises de l'Atlantique et de la Manche: réactualisation des données par la méthode des "sea-level index points". Quaternaire 25, 295–312.
Stéphan, P., Goslin, J., Pailler, Y., Manceau, R., Suanez, S., Van Vliet-Lanoë, B., Hénaff, A., Delacourt, C., 2015a. Holocene salt-marsh sedimentary infilling and relative sea-level changes in West Brittany (France) using foraminifera-based transfer functions. Boreas 44, 153–177.
Stéphan, P., Laforge, M., 2013. Mise au point sur l'évolution géomorphologique et le devenir des flèches de galets du Loc'h de Landévennec (Bretagne, France). Géomorphologie 19, 191–208.
Stéphan, P., Suanez, S., Fichaut, B., 2015b. Long-, mid- and short-term evolution of coastal gravel spits of Brittany, France. In: Randazzo, G., Jackson, D.W.T., Cooper, J.A.G. (Eds.), Sand and Gravel Spits. Springer, Cham, pp. 275–288.
Stuiver, M., Reimer, P.J., Reimer, R.W., 2017. CALIB 7.1. WWW program. http://calib.org/. (Accessed 8 September 2017).
Tastet, J.-P., Roussot-Larroque, J., Clavé, B., 2000. Palaeo-environmental study area P15: west bank of the Gironde estuary, west coast, France. In: McInnes, R.G., Tomalin, D.J., Jakeways, J. (Eds.), LIFE Environment Project: LIFE-97 ENV/UK/000510 1997-2000 Coastal Change, Climate and Instability: Final Technical Report. Isle of Wight Center for the Coastal Environment, Newport. Dir.
Teixeira, S.B., Gaspar, P., Rosa, M., 2005. Holocene sea-level index points on the Quarteira coast (Algarve, Portugal). In: Freitas, M.C., Drago, T. (Eds.), Iberian Holocene Paleoenvironmental Evolution. Proceedings Coastal Hope Conference 2005. Universidade de Lisboa, Lisboa, pp. 125–127.
Terrinha, P.A.G., 1998. Structural Geology and Tectonic Evolution of the Algarve Basin, South Portugal. Ph.D. thesis. Imperial College London.
Tisnérat-Laborde, N., Paterne, M., Métivier, B., Arnold, M., Yiou, P., Blamart, D., Raynaud, S., 2010. Variability of the northeast Atlantic sea surface Δ14C and marine reservoir age and the North Atlantic Oscillation (NAO). Quat. Sci. Rev. 29, 2633–2646.
Tooley, M.J., 1982. Sea-level changes in northern England. Proc. Geol. Assoc. 93, 43–51.
Törnqvist, T.E., Hijma, M.P., 2012. Links between early Holocene ice-sheet decay, sea-level rise and abrupt climate change. Nat. Geosci. 5, 601–606.
Törnqvist, T.E., Wallace, D.J., Storms, J.E.A., Wallinga, J., van Dam, R.L., Blaauw, M.,

Derksen, M.S., Klerks, C.J.W., Meijneken, C., Snijders, E.M.A., 2008. Mississippi Delta subsidence primarily caused by compaction of Holocene strata. Nat. Geosci. 1, 173–176.
Trog, C., Hempel, R., Frenzel, P., Mausbacher, R., 2015. Holocene palaeoenvironmental changes in three lagoons on the Algarve coast of Portugal. Palaeobiodivers. Palaeoenviron. 95, 203–221.
Trog, C., Höfer, D., Frenzel, P., Camacho, S., Schneider, H., Mäusbacher, R., 2013. A multi-proxy reconstruction and comparison of Holocene palaeoenvironmental changes in the Alvor and Alcantarilha estuaries (southern Portugal). Rev. Micropaleontol. 56, 131–158.
Ullman, D.J., Carlson, A.E., Hostetler, S.W., Clark, P.U., Cuzzone, J., Milne, G.A., Winsor, K., Caffee, M., 2016. Final Laurentide ice-sheet deglaciation and Holocene climate-sea level change. Quat. Sci. Rev. 152, 49–59.
Vacchi, M., Marriner, N., Morhange, C., Spada, G., Fontana, A., Rovere, A., 2016. Multiproxy assessment of Holocene relative sea-level changes in the western Mediterranean: sea-level variability and improvements in the definition of the isostatic signal. Earth Sci. Rev. 155, 172–197.
van Asselen, S., Stouthamer, E., van Asch, T.W.J., 2009. Effects of peat compaction on delta evolution: a review on processes, responses, measuring and modeling. Earth Sci. Rev. 92, 35–51.
van de Plassche, O., 1986. Sea-level Research: a Manual for the Collection and Evaluation of Data. Geobooks, Norwich).
Vis, G.-J., Kasse, C., 2009. Late Quaternary valley-fill succession of the lower Tagus Valley. Portugal. Sediment. Geol. 221, 19–39.
Vis, G.-J., Kasse, C., Vandenberghe, J., 2008. Late Pleistocene and Holocene palaeogeography of the Lower Tagus Valley (Portugal): effects of relative sea level, valley morphology and sediment supply. Quat. Sci. Rev. 27, 1682–1709.
Ward, S.L., Neill, S.P., Scourse, J.D., Bradley, S.L., Uehara, K., 2016. Sensitivity of palaeotidal models of the northwest European shelf seas to glacial isostatic adjustment since the Last Glacial Maximum. Quat. Sci. Rev. 151, 198–211.
Whitehouse, P.L., Bentley, M.J., Le Brocq, A.M., 2012. A deglacial model for Antarctica: geological constraints and glaciological modelling as a basis for a new model of Antarctic glacial isostatic adjustment. Quat. Sci. Rev. 32, 1–24.